Theory of Thomson Scattering of Partially Coherent Laser Probes in Plasmas

by

Mehraveh Javan Roshtkhari

A thesis submitted in partial fulfillment of the requirements for the degree of

Master of Science

Department of Physics
University of Alberta

Abstract

The effect of partial coherence of a probe on the spectrum of Thomson scattered radiation from plasma is investigated. The coherence of a probe is described in terms of the electric field Gaussian correlation function of the finite correlation time (longitudinal coherence) and the finite correlation length (transverse coherence). The Thomson scattering cross section is defined using dynamical form factor, i.e. Fourier transformed correlation function of electron density fluctuations. Two limiting cases of spatial (very large correlation length) and temporal (very long correlation time) coherence are considered. Thomson spectra of scattered radiation are calculated for these two cases and analyzed in the regime of collective plasma response dominated by ion-acoustic and Langmuir wave fluctuations. Partial coherence of the probe (finite coherence time and length) alters the scattered spectrum significantly. Two examples are discussed for each case by varying these two parameters of the correlation function. Finally, using inverse Fourier transforms, a theory is developed to show the possibility of recovering ion acoustic fluctuation spectrum from the scattered light spectrum of the partially coherent pump.

Acknowledgements

I would like to express my gratitude to my supervisor Dr. Wojciech Rozmus for the opportunity to conduct this research, and for his guidance, encouragement and support during the past two years.

I would like to thank committee members Dr. Richard Sydora and Dr. Ying Tsui for assistance and suggestions they provided.

Special thanks go to Dr. Richard Marchand and all the professors who ever taught me for their help and encouragement during my study at the University of Alberta.

Last but not the least, I would like to thank all my family and friends for their support in various forms.

Contents

List of Tables

List of Figures

Chapter 1

Introduction

Thomson scattering is one of the most widely used diagnostic methods for plasma. The aim of this thesis is to investigate the effect of a partially coherent laser probe on the Thomson scattering spectrum of a plasma. To achieve this goal, a connection needs to be established between properties of the probe and the scattered radiation spectrum. In this introductory chapter, basic concepts of plasma physics which are essential to understanding of the rest of thesis, are reviewed. Furthermore, other plasma diagnostic techniques are also briefly reviewed. The subject and content of other chapters are reviewed in section 1.5.

Prior to any calculation in this work, it is important to establish the units of physical quantities used. In agreement with plasma physics literature and research, temperature is expressed in units of energy electron volts (eV). The conversion factor is $1eV = 11600K$, where K stands for Kelvins.

To distinguish vectors from scalars, bold format is used for vectors. All theoretical calculations are carried out in Gaussian systems of units. For more information about conversion between Gaussian and SI systems of units see [1]. Maxwell equations in medium in Gaussian units are:

$$\nabla \times \mathbf{E} = -\frac{1}{c}\frac{\partial \mathbf{B}}{\partial t} \tag{1.1}$$

$$\nabla \times \mathbf{H} = \frac{4\pi}{c}\mathbf{J} + \frac{1}{c}\frac{\partial \mathbf{D}}{\partial t} \tag{1.2}$$

$$\nabla \cdot \mathbf{D} = 4\pi\rho \tag{1.3}$$

$$\nabla \cdot \mathbf{B} = 0 \tag{1.4}$$

And Lorentz force on charge q moving with velocity $\mathbf{v}$ and subject to electric field $\mathbf{E}$ and magnetic field $\mathbf{B}$ is:

$$\mathbf{F} = q(\mathbf{E} + \frac{\mathbf{v} \times \mathbf{B}}{c}) \tag{1.5}$$

1.1 Plasma Physics Review

Historically, plasma research has its roots in the study of gas discharges. In fact the term "plasma", was used in 1928 by Langmuir [2] to describe the ionized state of a gas in an arch discharge. Although, it was observed before, as early as 1879 by William Crookes [3] and later identified by Thomson [4]. The existence of the ionosphere was theorized in eighteenth century by Carl Gauss and proved in 1920s [5]. The role of the ionosphere in radio broadcasting and the discovery that plasma is an important component of the universe, intensified the interest in plasma physics. In 1950s, the research was more focused on controlled fusion as a possible energy source and with the development of lasers in 1960s, the new field of laser-plasma physics was created [6].

A plasma is a statistical system containing mobile electrons and ions. Inside plasma, local charge imbalance can be present providing the source for electromagnetic fields. However, plasma is overall quasi-neutral, i.e. number of negative and positive charges are equal. The key features of plasma are quasi-neutrality, mobility and collective behavior of charges. Collective behavior is

the result of long range electromagnetic forces in plasma.

Two theories are used to describe plasma: fluid theory and kinetic theory. The former is simpler, where plasma is treated as a conducting fluid and equations of fluid mechanics are used. Although more complicated, the latter is more adequate in describing plasma phenomena.

1.1.1 Characteristic Quantities in Plasma

Mobility of charges in plasma means that they have the ability of screening interactions of other charges. Debye shielding is an effect where a charge in a plasma is shielded by other charges over a characteristic length λ_D. In other words, the charges redistribute themselves so as to shield the plasma from the electric field that perturbs the plasma. The electron Debye length is defined as:

$$\lambda_D = \sqrt{\frac{T_e}{4\pi n_e e^2}} \tag{1.6}$$

Using Debye length, quasi-neutrality is satisfied if the dimensions of system is much larger than λ_D.

Another important parameter is plasma frequency, ω_p. In a plasma with a uniform background of ions, electrons displaced from their equilibrium position oscillate with frequency ω_p which only depends on plasma density. This frequency can be derived by solving linearized equations of motion of electron, continuity and Poisson's equations resulting in:

$$\omega_p = \sqrt{\frac{4\pi n_e e^2}{m_e}} \tag{1.7}$$

1.2 Plasma Diagnostic Methods

The overall objective of plasma diagnostics is to deduce information about the state of the plasma from practical observations of physical processes and their effects. The first observations were of glows in gas discharge tubes. The discovery of electrons, ions, and later the ionizing effects of x-rays, caused the expansion of the field in the twentieth century. The first methods used electrostatic probes for diagnosing the plasma. The advancements in quantum mechanics led to the use of spectroscopy in plasma diagnostics [7].

In general, diagnostics methods can be categorized as below [8]:

Magnetic measurements: Made by directly measuring magnetic field in various places inside and outside the plasma, using coils and probes of various types

Particle flux measurements: Based on directly measuring the flux of plasma particles, using probes of various types in contact with plasma

Refractive index: Measurements of plasma's refractive index for electromagnetic waves of appropriate wavelength by measuring transmission through plasma

Scattering of electromagnetic waves: Measurements of the scattered radiation by plasma subject to an incident radiation

Optical emission: From free electrons, observing the emitted radiation including cyclotron emission and Bremsstrahlung; and from bound electrons, observing the line radiation from ions

In [8] one can find more detailed description of each method, although it emphasizes diagnostics of fully ionized plasmas. Also, [9] focuses on methods for the investigation of low-temperature plasmas.

Scattering of the electromagnetic wave by plasma is one of the most powerful diagnostic methods because of two main features: first, it is a non-perturbing method which has a significant advantage over electrostatic probe methods. Second, it has the potential to provide detailed information about properties of electrons (and sometimes even ions too), such as density and temperature [8]. However, due to the weak signal of scattered radiation measured in experiments, the scattering method could not be used for laboratory plasma diagnostics until lasers were invented [9].

1.3 Scattering of Light by Matter

The first phenomena of scattering of light from plasma to be studied was the reflection of radio waves from the ionosphere. In the earliest scattering experiments, microwaves were usualy used. Reference [10] provides a detailed review of work on scattering of radiation from plasma.

This method of diagnostics is of special interest due to its ability to provide direct measurements of local plasma parameters. In this method the scattered radiation is observed from a small volume intersecting the light beam, probing the plasma with a cone within which, the radiation scattered by the plasma is recorded. The spectrum of the scattered radiation strongly depends on plasma parameters.

Light scattering (electromagnetic wave scattering) can be categorized as elastic or inelastic scattering. In elastic scattering the energy transfer is negligible, while in inelastic scattering it is not. Elastic scattering mainly includes Rayleigh (and Mie) scattering and Thomson scattering while Compton scattering is inelastic scattering. In sections 1.3.1, 1.3.2 and 1.3.3, Rayleigh, Thomson and Compton scatterings are briefly discussed.

1.3.1 Rayleigh Scattering

One of the first studies on the scattering of electromagnetic waves was carried out by John Tyndall in 1869. He was trying to explain the blue color of the sky and he found that the color was due to the scattering of the sun's light from small dust particles in the atmosphere (called Tyndall effect). The scattering of light from gas molecules was further investigated in 1871 by Lord Rayleigh [11].

Rayleigh scattering is elastic scattering of light from particles occurring only when the size of the scatterer is considerably smaller than the wavelength of the incident radiation. In plasma, this means scattering of photons from heavy particles (neutrals and ions). Because the interaction is elastic, neither particle nor photon experiences a change in energy and the scattered light maintains the incident wavelength.

Introducing ς as the size parameter:

$$\varsigma = \frac{2\pi a}{\lambda_0} \tag{1.8}$$

where a is the size of the scatterer and λ_0 is the probe wavelength; for Rayleigh scattering to occur $\varsigma << 1$.

In case the size of the scatterer is comparable to the wavelength ($\varsigma \approx 1$) the scattering is called Mie scattering (also known as Mie solution to Maxwell equation or Lorenz-Mie solution). This is named after German physicist Gustav Mie, who described the scattering of an electromagnetic plane wave by a homogeneous sphere in 1908. Geometric scattering happens if the size of the scatterer is much larger than the wavelength ($\varsigma >> 1$). Detailed account of Rayleigh scattring can be found in many textbooks including reference [12] which also provides a short account of Mie scattering.

Rayleigh scattering can be used to determine the temperature and density of ions in the plasma, in the same way that Thomson scattering is used for

electrons. In [9] the method of using Rayleigh scattered light to determine the concentration and temperature of heavy particles is described. Rayleigh scattering is also used for calibration in diagnostics experiments [10].

1.3.2   Thomson Scattering

The process of the scattering of electromagnetic radiation from free electrons is named after English physicist J. J. Thomson, who studied the phenomena in 1904.

When electromagnetic wave interacts with a free electron, the oscillating electric and magnetic fields of the wave exert a Lorentz force on the electron. This causes the electron to accelerate and emit radiation in all directions. Due to the motion of the electrons, the scattered light is Doppler shifted and this change in the frequency of scattered light can provide information about kinetic properties of electrons.

The description above is purely classical. However, Thomson scattering can be approached from a quantum mechanical point of view by describing the process as the collision of photons with the particles. If the change in the momentum of the particle is negligible, this will lead to the same results as the classical approach. In this case the photon energy should be much smaller than the electron rest energy and we should have $h\nu << m_e c^2$. If this limit is not satisfied, the results will be different and the situation is called Compton scattering, which is briefly discussed in 1.3.3. Therefore, Thomson scattering is in fact the classical limit of Compton scattering.

The electron temperature is obtained by measuring the spectral width of the Thomson scattered radiation and the density is obtained by measuring its intensity. The Thomson scattering cross section is proportional to the number of electrons in the scattering volume. The Doppler shift depends on the velocities of the electrons; therefore, a measurement of the frequency of the scattered light can theoretically provide information on the velocity distribution of the

electrons. From this, the electron temperature in the plasma can be evaluated. However, as it is difficult to determine the precise shape of the electron velocity distribution from experimental data; a specific Maxwellian distribution is often chosen and fitted to the scattered spectrum to infer the electron temperature. Thomson scattering is described in more detail in chapter 2.

Although most Thomson scattering measurements have been performed using lasers, the earliest application of Thomson scattering as a diagnostic method was a density measurement in the ionosphere using radars. The technique was suggested by Gordon [13] and the first observations were reported by Bowles [14], followed by Pineo et al. [15] [10].

In 1963, the first experimental observation of Thomson scattering from free electrons was reported by Fiocco and Thomson [16], using a Ruby laser interacting with an electron beam. The first demonstration of Thomson Scattering as a suitable diagnostic tool for hot plasmas was given by Peacock et al. in 1969, when they measured the electron temperature and density in the Russian T3 tokamak [17]. The proliferation of lasers made Thomson scattering a widespread diagnostic tool in plasma physics, especially in the fusion community.

Because of the high electron density and temperature of fusion plasmas, they are capable of producing a strong Thomson scattering signal. Therefore, since the late 1960s, Thomson scattering has been a part of fusion research.

1.3.3   Compton Scattering

In 1922, Arthur Compton was studying the scattering of X-rays by a thin foil of graphite. He observed that the scattered X-ray has a longer wavelength compared to the incident wave, which was inconsistent with the predictions from the Thomson scattering theory [18]. The wavelength shift depended on the scattering angle θ as:
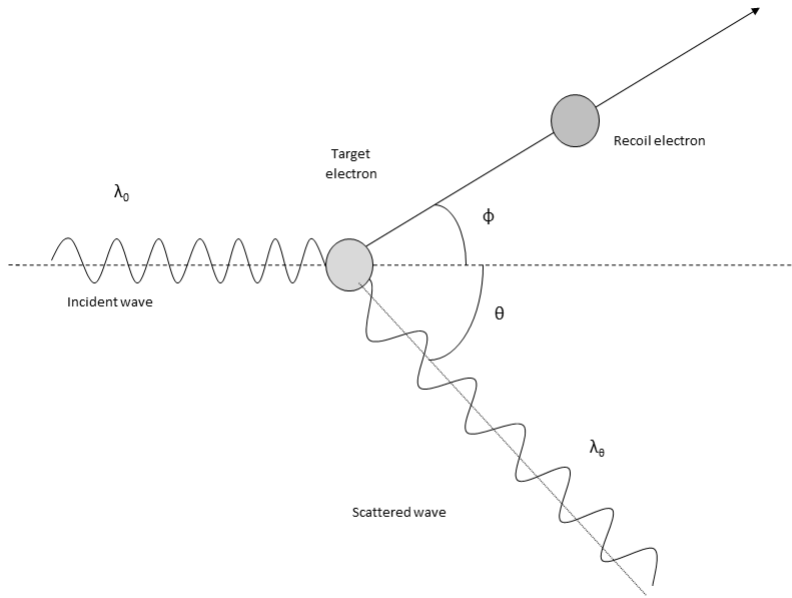
Figure 1.1: Compton scattering of a photon with wavelength λ_0, detection at angle θ

$$\lambda_\theta - \lambda_0 = \frac{h}{m_e c}(1 - cos(\theta)) \tag{1.9}$$

where λ_θ is the scattered wavelength at angle θ with respect to the incident wave with wavelength λ_0 (see figure 1.1).

Compton successfully explained his observation by considering the particle nature of light and applying momentum and energy conservation to the collision between a photon and a stationary electron. In this process, some part of the energy of the incident photon is transferred to the electron, causing it to recoil as seen in figure 1.1; therefore the scattered photon has less energy. Compton scattering of an electron and a photon can be found in many books including [1].

This was an important scientific discovery because although at that time the particle nature for light was already suggested to explain the photoelectric

effect, the subject was under debate. Compton's discovery provided clear evidence to the particle-like behavior of light and earned him a Nobel Prize in 1927.

Compton Scattering is the earliest example of inelastic scattering and is only significant when the incident energy of photon is comparable to the rest energy of the electron ($m_e c^2$). Compton also discovered that a photon can gain (rather than lose) energy from a relativistic electron. This feature is called inverse Compton scattering and the frequency of the scattered radiation can be as high by the factor of γ^2 of incident wave; where γ is the Lorentz factor of the electrons [19]. Inverse Compton Scattering was recognized in 1963 as a very useful mechanism to produce high energy x-ray and γ-ray beams [20] [21].

1.4   Aim and Objectives

The objective of this thesis is to investigate the effects of probe incoherence on Thomson scattered spectrum of a plasma. In this process, we review Thomson scattering process and discuss different scattering regimes (collective and noncollective). By deriving the scattered power for a random probe, we show the connection of scattered spectrum to the probe electric field correlation function. Then, optical coherence theory is reviewed to find the electric field correlation function and explain its link to partial coherence. Using fundamental plasma physics and electrodynamics, the dynamic form factor (Fourier transformed correlation function of electron density fluctuations) is then established.

1.5   Chapter Overview

Chapter 2: Thomson Scattering Basics of Thomson scattering is discussed. Radiation from a moving charge is reviewed and Thomson scattering cross section is derived. Collective and noncollective scattering is reviewed.

Chapter 3: Optics of the probe Random light processes and spatial and temporal coherence are discussed. Gaussian correlation function for partially coherent light is derived.

Chapter 4: Dressed Test Particle and Plasma Form Factor Starting from Klimontovich equation, dressed test particle model is used to derive dynamic form factor for Maxwellain plasma. Ion-accoustic and electron-plasma waves are discussed.

Chapter 5: Results Two limiting cases of longitudinal and transverse coherence are discussed. For each case, two examples are provided using MATLAB software. A method is discussed to demonstrate the possibility of recovering ion-acoustic waves in case of probe's spatial coherence.

Chapter 6: Summary and Conclusions Summary of thesis, interpretation of findings, limitations of models and suggestions.

Chapter 2

Thomson Scattering

As discussed in previous chapter, Thomson scattering is the scattering of radiation from free electrons. Therefore in this chapter radiation by a moving charge is discussed first. Then, Thomson cross section and Doppler shift of the incident wave are derived. The generalization is made for plasma and dynamic form factor and collective and noncollective regimes of scattering are discussed.

2.1 Radiation from a Moving Charge

To determine what happens to an electron accelerated in the electric field of a laser, one must start with Maxwell's equations (1.1) to (1.4). The solution to Maxwell equations in this case are the well known Liénard-Wiechert potentials. Detailed solutions can be found in many electrodynamics text books, such as [1] and [22].

For vector potential $\mathbf{A}$ and potential ϕ we have:

$$\mathbf{E}(\mathbf{r}, t) = -\bigtriangledown \phi - \frac{\partial \mathbf{A}}{\partial t} \tag{2.1}$$

$$\mathbf{B}(\mathbf{r}, t) = \bigtriangledown \times \mathbf{A} \tag{2.2}$$
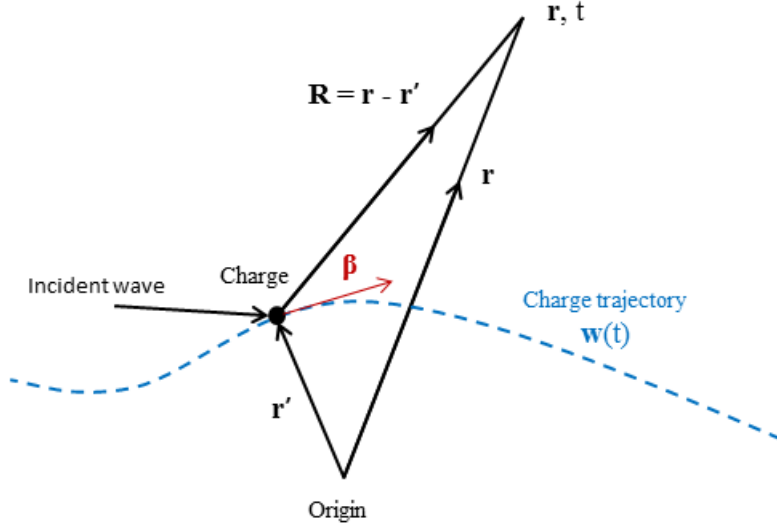
Figure 2.1: Scattering coordinates

Substitution of equations (2.1) and (2.2) in the Maxwell equations, results in Maxwell's equations in the potential formulation. In Lorentz gauge, the solutions that satisfy them are the retarded potentials:

$$\mathbf{A}(\mathbf{r}, t) = \frac{1}{c} \int \frac{\mathbf{J}(\mathbf{r}', t_r)}{R} d^3 r' \tag{2.3}$$

$$\Phi(\mathbf{r}, t) = \int \frac{\rho(\mathbf{r}', t_r)}{R} d^3 r' \tag{2.4}$$

Where $\mathbf{r}'$ is the position of the charge (see figure 2.1), and:

$$\mathbf{R} = \mathbf{r} - \mathbf{r}' \tag{2.5}$$

$\mathbf{J}$ is the current density and ρ is the charge density and the potentials are related to the behavior of ρ and $\mathbf{J}$ at retarded time t_r:

$$t_r = t - \frac{R}{c} \tag{2.6}$$

For a single point charge particle q we have:

$$\rho(\mathbf{r}', t) = q\delta^3(\mathbf{r}' - \mathbf{w}(t)) \tag{2.7}$$

where $\mathbf{w}(t)$ is the trajectory of the particle. At retarded time we can write:

$$\rho(\mathbf{r}', t_r) = \int \rho(\mathbf{r}', t')\delta(t' - t_r)dt' \tag{2.8}$$

Substituting (2.8) and (2.7) into (2.4) we have:

$$\Phi(\mathbf{r}, t) = \int\int \frac{q}{R}\delta^3(\mathbf{r}' - \mathbf{w}(t'))\delta(t' - t_r)dt'd^3r' \tag{2.9}$$

Fields associated with these potentials are:

$$\mathbf{E}(\mathbf{r}, t) = q[\frac{(\widehat{\mathbf{s}} - \boldsymbol{\beta})(1 - \beta^2)}{(1 - \widehat{\mathbf{s}}\cdot\boldsymbol{\beta})^3 R^2}]_{ret} + [\frac{\widehat{\mathbf{s}}\times\{(\widehat{\mathbf{s}} - \boldsymbol{\beta})\times\dot{\boldsymbol{\beta}}\}}{(1 - \widehat{\mathbf{s}}\cdot\boldsymbol{\beta})^3 R}]_{ret} \tag{2.10}$$

$$\mathbf{B}(\mathbf{r}, t) = (\widehat{\mathbf{s}}\times\mathbf{E}) \tag{2.11}$$

where $\boldsymbol{\beta} = \mathbf{v}/c$ and $\widehat{\mathbf{s}} = \mathbf{R}/R$. Far from the source (radiation zone $r' \ll r$), the first term in equation (2.10) can be dropped. In the denominator, we make the approximation $R \approx r$. However, it is important to note that this approximation may not be made in the retarded time. Instead we can write: $R \approx r - \hat{\mathbf{s}}\cdot\mathbf{r}'$, and therefore:

$$t_r \approx t - \frac{|r - \widehat{\mathbf{s}}\cdot\mathbf{r}'|}{c} \tag{2.12}$$

Now considering low velocity charges (non-relativistic $\beta = |v/c| \ll 1$), equation (2.10) becomes:

$$\mathbf{E}(\mathbf{r}, t) = \frac{q}{cr}[\widehat{\mathbf{s}}\times(\widehat{\mathbf{s}}\times\dot{\boldsymbol{\beta}})]_{ret} \tag{2.13}$$

by using the Poynting vector:

14
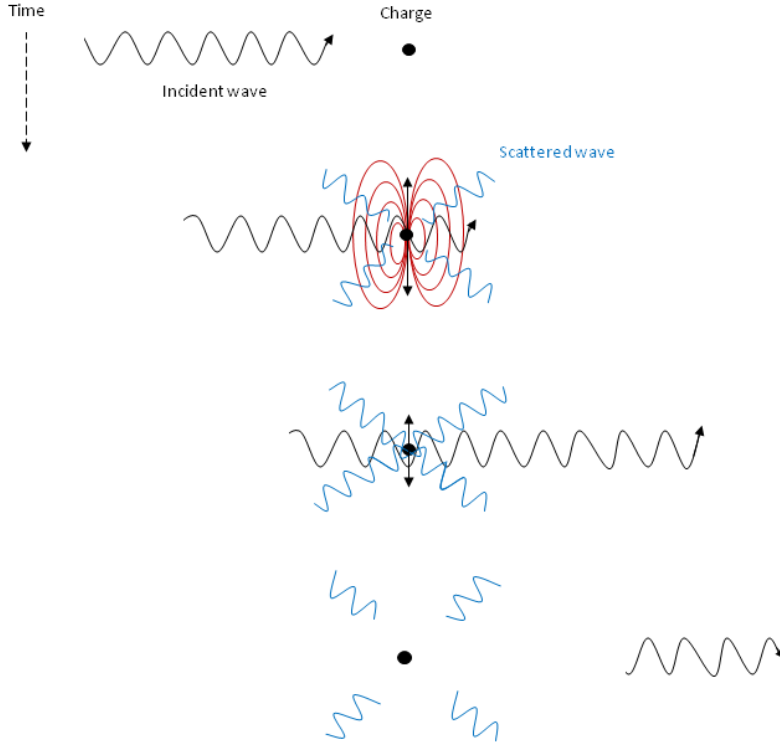
Figure 2.2: Scattering of electromagnetic radiation by a charge

$$\mathbf{S} = \frac{c}{4\pi}\mathbf{E} \times \mathbf{B} \tag{2.14}$$

one can find the the scattered power per unit solid angle:

$$\frac{dP_s}{d\Omega} = r^2\mathbf{S} \cdot \widehat{\mathbf{s}} = \frac{q^2}{4\pi}[\widehat{\mathbf{s}} \times (\widehat{\mathbf{s}} \times \dot{\boldsymbol{\beta}})]^2_{ret} \tag{2.15}$$

2.1.1 Scattering of Electromagnetic Wave by a Charge

Now, we assume that the moving charge is accelerated by an electromagnetic wave. As shown in figure 2.2, the fields accelerate the charge, which in turn emits radiation.

For simplicity, we consider the case of a plane monochromatic wave incident upon a charge q. For incident fields we have:

15

$$\mathbf{E_i}(\mathbf{r'}, t) = E_{i0}cos(\mathbf{k_i} \cdot \mathbf{r'} - \omega_i t) \tag{2.16}$$

$$\mathbf{B_i}(\mathbf{r'}, t) = \widehat{\mathbf{i}} \times \mathbf{E_i} \tag{2.17}$$

where E_{i0} is the amplitude and $\mathbf{k_i}$ and ω_i are incident wave vector and frequency and $\widehat{\mathbf{i}} = \mathbf{k_i}/k_i$. The charge will experience Lorentz force:

$$\mathbf{F} = q(\mathbf{E_i} + \frac{\mathbf{v}}{c} \times \mathbf{B_i}) \tag{2.18}$$

In [10] four different situations are considered, distinguishing between low velocity ($|v/c| \ll 1$) and high velocity charges and whether any additional force is present. Here, we only consider the first case, where we can neglect the effect of the magnetic field of the incident wave and equation of motion can be written as:

$$m(\frac{d\mathbf{v}}{dt}) = qE_{i0}cos(\mathbf{k_i}.\mathbf{r'} - \omega_i t) \tag{2.19}$$

The unperturbed trajectory of the particle is:

$$\mathbf{r'}(t_{ret}) = \mathbf{r'}(0) + \mathbf{v}t_{ret} \tag{2.20}$$

Substituting in equation (2.12) we have:

$$t_{ret} = \frac{t - r/c + (\widehat{\mathbf{s}} \cdot \mathbf{r'}(0))/c}{1 - \widehat{\mathbf{s}} \cdot \boldsymbol{\beta}} \tag{2.21}$$

Using dispersion relation for the incoming electromagnetic radiation:

$$\omega_i = ck_i \tag{2.22}$$

equations (2.20) and (2.21) result in:

$$\mathbf{k_i} \cdot \mathbf{r}' - \omega_i t_{ret} = [(r - \widehat{\mathbf{s}} \cdot \mathbf{r}'(0))k_i - \omega_i t]\frac{1 - \widehat{\mathbf{i}} \cdot \boldsymbol{\beta}}{1 - \widehat{\mathbf{s}} \cdot \boldsymbol{\beta}} + \mathbf{k_i} \cdot \mathbf{r}'(0) \qquad (2.23)$$

substituting in equation (2.19) and then in equation (2.13), the scattered electric field will be:

$$\mathbf{E_s}(\mathbf{r}, t) = \frac{q^2}{mrc^2}[\widehat{\mathbf{s}} \times (\widehat{\mathbf{s}} \times \mathbf{E_{i0}})]cos[k_s r - \omega_s t - (\mathbf{k_s} - \mathbf{k_i}) \cdot \mathbf{r}'(0)] \qquad (2.24)$$

where:

$$\omega_s = \omega_i \frac{1 - \widehat{i} \cdot \boldsymbol{\beta}}{1 - \widehat{s} \cdot \boldsymbol{\beta}} = \omega_i + \mathbf{k} \cdot \mathbf{v} \qquad (2.25)$$

and

$$\omega_s = ck_s \qquad (2.26)$$

From equation (2.25), it can be seen that the scattered radiation is frequency shifted as a double Doppler effect takes place: one in the reception, one in the emission of radiation by the electron. The numerator is caused by the photon approaching the moving charge, while the denominator is caused by the photon leaving the charge.

Conveniently, we can work in terms of frequency shift ω and scattering wave vector $\mathbf{k}$ (see figure 2.3):

$$\omega = \omega_s - \omega_i = \mathbf{k} \cdot \mathbf{v} \qquad (2.27)$$

$$\mathbf{k} = \mathbf{k_s} - \mathbf{k_i} \qquad (2.28)$$

From equation (2.27) it is obvious that (for $\beta \ll 1$) the Doppler shift is

17
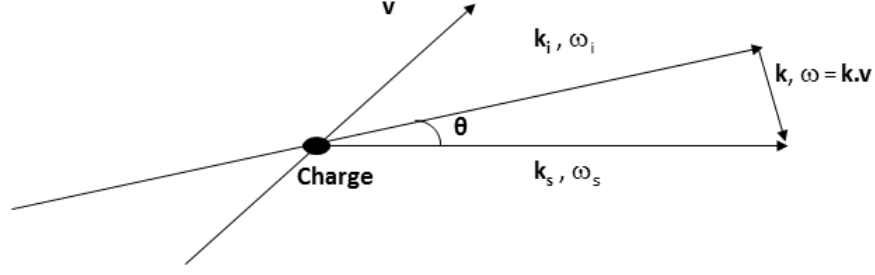
Figure 2.3: Frequency shift in Thomson scattering

directly proportional to the velocity of the particle along the scattering vector.

One could find these results alternatively by considering the conservation of energy and momentum. In the electron reference frame, conservation of energy reads:

$$\hbar\omega'_i + m_e c^2 = \hbar\omega'_f + \gamma_f m_e c^2 \tag{2.29}$$

where indexes i and f represent values for incident wave and scattered wave and $\gamma_f = 1/\sqrt{1 - \beta'_f{}^2}$. Conservation of momentum reads:

$$\hbar\mathbf{k}'_i = \hbar\mathbf{k}'_f + \gamma_f m_e c^2 \boldsymbol{\beta}'_f \tag{2.30}$$

From equation (2.30), γ_f can be found as:

$$\gamma_f = \sqrt{1 + \frac{\hbar^2}{m_e^2 c^2}(\mathbf{k}'_f - \mathbf{k}'_i)^2} \tag{2.31}$$

By using $k'_f \simeq k'_i$ and substitution of γ_f in equation (2.29), we find:

$$\hbar\omega'_i = \hbar\omega'_f + \frac{\hbar^2}{2m_e}(k'_f{}^2 + k'_i{}^2 - 2k'_f k'_i \cos(\theta)) \tag{2.32}$$

and

$$\omega'_f = \omega'_i \frac{1}{1 + \frac{\hbar\omega'_i}{m_e c^2}(1 - \cos(\theta))} \tag{2.33}$$

Going back to the observer reference frame reads:

18

$$\omega'_f = \omega_f \gamma_i (1 - \boldsymbol{\beta}_f \cdot \widehat{\mathbf{f}}) \tag{2.34}$$

and

$$\omega'_i = \omega_i \gamma_i (1 - \boldsymbol{\beta}_i \cdot \widehat{\mathbf{i}}) \tag{2.35}$$

Where $\gamma_i = 1/\sqrt{1 - \beta_i^2}$. Substitution of (2.35) and (2.34) in equation(2.33) and considering non relativistic scattering ($\beta \simeq 0$), reads Compton scattering frequency as:

$$\omega_f = \omega_i \frac{1}{1 + \frac{\hbar \omega_i}{m_e c^2}(1 - cos(\theta))} \tag{2.36}$$

which is equivalent to equation (1.9). Ignoring quantum effects $\hbar \omega_i \ll m_e c^2$, equation (2.33) then leads to:

$$\omega_s = \omega_i \frac{1 - \widehat{\mathbf{i}} \cdot \boldsymbol{\beta}_i}{1 - \widehat{\mathbf{s}} \cdot \boldsymbol{\beta}_f} = \omega_i + \mathbf{k} \cdot \mathbf{v} \tag{2.37}$$

which for $\boldsymbol{\beta}_i \simeq \boldsymbol{\beta}_f$ leads to the same result as equation (2.25).

2.1.2 Scattering by a Plasma

If the density of charges in the scattering volume is very low, the collective effect is insignificant and the radiated electric field can be found by adding Liénard-Wiechert potential of each charge. However, at higher plasma densities, emitted radiation is affected by the presence of other charges and particle correlations must be taken into account. For a plasma with density fluctuation δn, the microscopic current density $\mathbf{J}$ is:

$$\mathbf{J} = q\mathbf{v_e}\delta n \tag{2.38}$$

and in terms of $\mathbf{E_i}$ we have:

19

$$v_e = \frac{-ie}{m_e\omega_i}E_i \tag{2.39}$$

Substitution in equation (2.38) and taking time derivation leads to:

$$\frac{d\mathbf{J}}{dt} = \frac{e^2}{m_e}\mathbf{E_i}\,\delta n \tag{2.40}$$

In radiation zone, vector potential (2.3) can be written as:

$$\mathbf{A}(\mathbf{r},t) = \frac{1}{cr}\int d^3r' \int dt'\,\mathbf{J}\,\delta(t' - t + \frac{r}{c} - \frac{\widehat{\mathbf{s}}\cdot\mathbf{r}'}{c}) \tag{2.41}$$

Radiated fields in the radiation zone are [23]:

$$\mathbf{E_s}(\mathbf{r},t) = \frac{1}{c^2r}\int (\dot{\mathbf{J}}\times\widehat{\mathbf{s}})\times\widehat{\mathbf{s}}\ d^3r' \tag{2.42}$$

$$\mathbf{B_s}(\mathbf{r},t) = \frac{1}{c^2r}\int \dot{\mathbf{J}}\times\widehat{\mathbf{s}}\ d^3r' \tag{2.43}$$

From equation (2.39) it is clear that radiated fields depend on the incident electric field $\mathbf{E_i}$. Taking a general form for $\mathbf{E_i}$ as:

$$\mathbf{E_i}(\mathbf{r},t) = \frac{1}{2}\{\epsilon(\mathbf{r},t)\ exp(i\mathbf{k_0}\cdot\mathbf{r} - i\omega_0 t) + c.c.\} \tag{2.44}$$

where ϵ is a general random field satisfying the following:

$$\langle\epsilon\rangle = \langle\epsilon\cdot\epsilon\rangle = 0 \tag{2.45}$$

and,

$$\langle\epsilon\cdot\epsilon^*\rangle = C_{\epsilon\epsilon*}(\mathbf{r} - \mathbf{r}', t - t') \tag{2.46}$$

Ensemble average is denoted by $\langle...\rangle$ and $C_{\epsilon\epsilon*}(\mathbf{r} - \mathbf{r}', t - t')$ is the correlation function. These are discussed in Chapter 3. Defining:

$$\mathbf{E}(\mathbf{r}, t) =$$

$$-\frac{r_0}{2r} \int d^3r' \int dt' \, \delta(t' - t + \frac{r}{c} - \frac{\widehat{\mathbf{s}} \cdot \mathbf{r'}}{c}) \, \delta n(\mathbf{r'}, t') \, [\epsilon(\mathbf{r'}, t') \, exp(i\mathbf{k_0}.\mathbf{r'} - i\omega_0 t') + c.c.]$$

Equations (2.42) and (2.43) read:

$$\mathbf{E_s}(\mathbf{r}, t) = (\widehat{\mathbf{s}} \times \mathbf{E}) \times \widehat{\mathbf{s}} \tag{2.47}$$

$$\mathbf{B_s}(\mathbf{r}, t) = \widehat{\mathbf{s}} \times \mathbf{E}(\mathbf{r}, t) \tag{2.48}$$

For probe with polarization ϕ_0 and scattering angle θ, Poynting vector (2.14) is:

$$\mathbf{S} = \frac{c}{4\pi} \, \widehat{\mathbf{s}} \, \langle \mathbf{E} \cdot \mathbf{E} \rangle (1 - sin^2\theta \, cos^2\phi_0) \tag{2.49}$$

If probe is not polarized, the average can be taken over ϕ_0 which results in the replacement of term $cos^2\phi_0$ by $1/2$. To calculate the term $\langle \mathbf{E} \cdot \mathbf{E} \rangle$, we note that if density fluctuations δn and probe electric field amplitude ϵ are statistically independent, the average can be separated into two correlation functions. Using equation (2.46):

$$\langle \delta n(\mathbf{r}, t) \, \delta n(\mathbf{r'}, t') \, \epsilon(\mathbf{r}, t) \cdot \epsilon^*(\mathbf{r'}, t') \rangle = \langle \delta n(\mathbf{r}, t) \, \delta n(\mathbf{r'}, t') \rangle \, C_{\epsilon\epsilon*}(\mathbf{r} - \mathbf{r'}, t - t') \tag{2.50}$$

Defining dynamic form factor $S(\mathbf{k}, \omega)$ as the Fourier transformation of $\langle \delta n(\mathbf{r}, t) \delta n(\mathbf{r'}, t') \rangle$ and using conditions of equations (2.27) and (2.28), scattered power per unit solid angle Ω, per spectral width $d\lambda$ is found to be:

$$\frac{dP_s}{d\Omega \, d\lambda} = \frac{c}{8\pi} \, (1 - \frac{1}{2}sin^2\theta) \frac{1}{2} n_e r_0^2 \frac{2\pi c}{\lambda^2} \, S * (C_{\epsilon\epsilon*} + C_{\epsilon*\epsilon}) \tag{2.51}$$

21
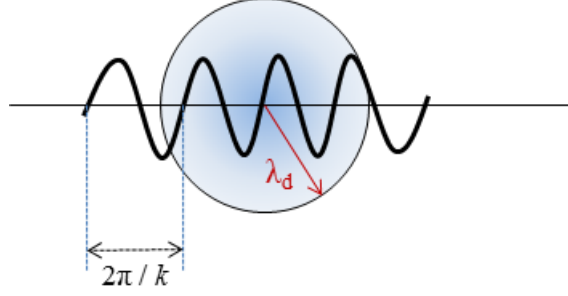
Figure 2.4: Non-collective scattering schematic with $\alpha \ll 1$
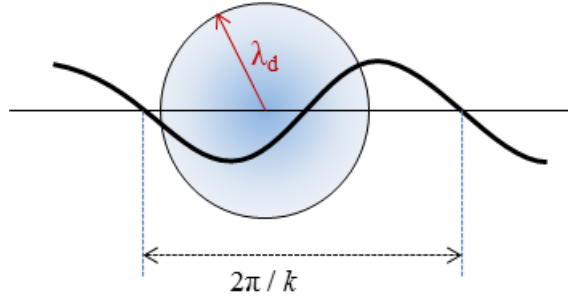
Figure 2.5: Collective scattering schematic with $\alpha \succeq 1$

where $S * C_{\epsilon\epsilon^*}$ is the convolution of form factor and correlation function:

$$S * C_{\epsilon\epsilon^*} = \int \frac{d^3 k'}{(2\pi)^3} \int \frac{d\omega'}{2\pi} \, S(\mathbf{k} - \mathbf{k}', \omega - \omega') \, C_{\epsilon\epsilon^*}(\mathbf{k}', \omega') \tag{2.52}$$

The derivation of correlation function and dynamic form factor are discussed in chapters 3 and 4 respectively.

2.2 Collective and Non-collective Scattering

A physical process that determines whether scattering is collective or non-collective is Debye shielding. Introduced by Sapleter [24], the scattering parameter α is defined as:

$$\alpha = \frac{1}{k\lambda_D} \tag{2.53}$$

and is a good indicator of the scattering regime. The perturbing effects of a charge will tend to penetrate into plasma at distances only on the order of the Debye length. When the wavelength of density fluctuations is short compared to the Debye length, the scattering from electrons in the scattering volume is randomly distributed and the scattering is said to be non-collective. This situation corresponds to $\alpha \ll 1$ (see figure 2.4) and the spectrum reflects the thermal motion of electrons and usually Maxwellian-like distribution of electron velocities.

For values of $\alpha \approx 1$ and larger (see figure 2.5), the scattering depends on the collective behavior of the electrons. Electron density fluctuations are dominated by the long wavelength perturbations including high frequency Langmuir waves and ion-accoustic modes that involve ion dynamics.

Chapter 3

Optics of the Probe

3.1 Introduction

Traditionally, optical properties of the Thomson probe are studied in an entirely deterministic framework. That means all physical quantities(such as the electric field) are described by mathematical functions that are fully specified. Although this approach is very useful in many cases, it fails to explain certain phenomena arisen from random fluctuations in optical fields. The properties of this random light is the subject of statistical optics which alongside geometrical optics, wave optics and quantum optics comprise the main branches of optics [25].

Unpredictable fluctuations of a light source or the medium which the light propagates through can set the rise of randomness in light. In fact, statistical phenomena are plentiful in optics; because of the fundamentally statistical attributes of the mechanism that create light. For example, natural light or the light radiated by a thermal source, is random because it is the result of superposition of independent radiation from a large number of atoms, with radiations having different frequency and phase. Another source of randomness can be the result of scattering from rough surfaces or a turbulent fluid [26]. Furthermore, other sources such as fluctuations in the index of refraction of the

transmitting media or wave front deformation due to focusing can contribute to the randomness of light [27].

Random light fields have been studied from the time of Newton. At first, the light scattered from rough surfaces such as the sea was seen to form random intensity pattern (named speckles) even showing various colors [28]. In nineteenth century, Lord Rayleigh solved many fundamental statistical problems related to optics and acoustics. Later, the discovery of the quantum nature of light and statistical interpretation of quantum mechanics increased the need for a statistical approach to optics [27].

Two important manifestation of randomness in light are optical coherence and optical polarization. The theory of coherence which has its root in Young's well known interference experiment, was explained by Max Born and Emile Wolf (reference [29]) after the publishing of Principles of Optics [26].

For an ideal source, i.e. a point source emitting spherical monochromatic light, the properties of the beam at any point in space and any time are predictable and the beam is perfectly coherent. Real sources however, have finite extensions in space and a finite spectral bandwidth and these factors cause disturbances in fields. Therefore, the waves emitted by real sources are only partially coherent. However ,lights sources with relatively narrow bandwidth such as sodium, mercury and cadmium lamps and single mode lasers are available. The light with narrow bandwidth $\Delta\omega$ and mean frequency $\overline{\omega}$ that satisfies:

$$\frac{\Delta\omega}{\overline{\omega}} \ll 1 \tag{3.1}$$

is called quasi-monochromatic light. For such light it can be shown by using Fourier analysis that amplitude and phase vary slowly over time periods $\Delta t \ll \frac{2\pi}{\Delta\omega}$ [30].

The first investigation related to the subject of partial coherence was done in 1865 by french physicist Émile Verdet by studying the interference pattern of the sunlight from two pinholes [29]. Considering the coherence as the ability

of light to interfere, in 1938 Zernike introduced degree of coherence in terms of the visibility of fringes produced by Young experiment. Today, coherence is defined by correlation properties of optical fields.

In the next sections, we will first define statistical average and then investigate two coherence domains; temporal and spatial coherence. Finally we develop the partially coherent Gaussian beam.

3.2 Random Processes and Correlation Function

As mentioned before for a perfectly coherent light, the temporal and spatial dependence of wave (electric and magnetic fields of an electromagnetic wave) is periodic and predictable. However, for random light, one should use statistical methods to describe the light since electromagnetic field dependence is not completely predictable. Figure 3.1 shows the time dependence of a coherent wave, the frequency of the wave is constant(monochromatic) while for random light it is not. To describe random light, one must use the fact that since random functions satisfy a wave equation (or Maxwell equations) and boundary conditions; the statistical average of them, including correlation functions must also satisfy these conditions [26]. Now one must define these averages and use them to classify light by its coherence.
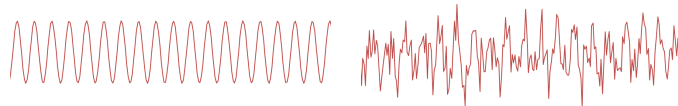

Figure 3.1: Time dependence of coherent and random wave amplitude

Defining an arbitrary wavefunction $u(\mathbf{r}, t)$ as the real part of complex wavefunction $U(\mathbf{r}, t)$; the intensity of deterministic light is:

$$I_m(\mathbf{r}, t) = U(\mathbf{r}, t)U^*(\mathbf{r}, t) \tag{3.2}$$

We know that for monochromatic light (unlike pulsed light) this value is independent of time. For random light $U(\mathbf{r}, t)$ and subsequently $I_m(\mathbf{r}, t)$ is random and called random or instantaneous intensity. Now imagine if a series of experiments is conducted in which the wave is produced (or measured) repeatedly under the same conditions. Randomness of wave means each time, there will be a random deviation from a mean value and hence each trial will produce a random wavefunction. Now there exist an ensemble of realizations of the random function $U(\mathbf{r}, t)$. The average intensity can now be defined by taking an average over the ensemble:

$$I(\mathbf{r}, t) = \langle U(\mathbf{r}, t)U^*(\mathbf{r}, t)\rangle \tag{3.3}$$

In general, if statistical averages of a random process' statistical properties (including intensity) are time invariant, then it is called a stationary random process. If for a stationary random process, the time average of statistical properties over the interval $-\infty < t < \infty$ are equal to the ensemble average of those properties; the process is called ergodic [30]. For random light, the time average is defined:

$$I(\mathbf{r}) = \lim_{T \to \infty} \frac{1}{2T} \int_{-T}^{T} U(\mathbf{r}, t)U^*(\mathbf{r}, t)dt \tag{3.4}$$

For a complex random function depending on time $f(t)$, the auto-correlation function is defined as:

$$C(t_1, t_2) = \langle f(t_1)f^*(t_2)\rangle \tag{3.5}$$

If the process is statistically stationary then the auto-correlation is only dependent on the time difference $\tau = t_2 - t_1$:

$$C(\tau) = \langle f(t)f^*(t+\tau) \rangle \tag{3.6}$$

Equation (3.6) is also called the temporal coherence function, because it is used to find the degree of temporal coherence.

Now considering $U(\mathbf{r}, t)$ which is a function of both position and time, we have mutual coherence function (second degree coherence phenomenon):

$$C(\mathbf{r_1}, \mathbf{r_2}, \tau) = \langle U(\mathbf{r_1}, t)U^*(\mathbf{r_2}, t+\tau) \rangle \tag{3.7}$$

It is clear that equation (3.6) is a special case of equation (3.7) for $\mathbf{r_1} = \mathbf{r_2}$. Therefore, two different limits can be distinguished; the first one being the case of a wave interfering with the time shifted version of itself ($\tau \neq 0$ and $\mathbf{r_1} = \mathbf{r_2}$) which leads to equation (3.6) and is related to temporal coherence which is discussed in section 3.3. The second case is the limit $\tau = 0$ and $\mathbf{r_1} \neq \mathbf{r_2}$ which results in:

$$C(\mathbf{r_1}, \mathbf{r_2}, t) = \langle U(\mathbf{r_1}, t)U^*(\mathbf{r_2}, t) \rangle \tag{3.8}$$

This is mutual intensity and for a statistically stationary light it is time independent and is often shown as $C(\mathbf{r_1}, \mathbf{r_2})$. This is discussed in section 3.4. For $\mathbf{r_1} = \mathbf{r_2} = \mathbf{r}$, equation (3.8) will simply give equation (3.3) which is the intensity of light at point $\mathbf{r}$. For statistically stationary light the intensity is time independent:

$$I(\mathbf{r}) = \langle U(\mathbf{r}, t)U^*(\mathbf{r}, t) \rangle \tag{3.9}$$

3.3   Temporal Coherence

In discussing temporal coherence, one is concerned with the ability of light to interfere with the time delayed version of itself, without being spatially shifted.

Michelson introduced a technique for measuring the temporal coherence using the set up now called Michelson interferometer [25]. Equation (3.6) is the correlation of one point in space at two different instants at time. This is proportional to the contrast of fringes in the Michelson interferometer and it's Fourier transform in time provides information regarding the spectral energy distribution of the light source [31].

If a quasi-monochromatic stationary beam of light with spectral bandwidth of $\Delta\omega$ is split and one component is time delayed by Δt (or path difference of $c\,\Delta t$) by means of Michelson interferometer for instance; one can understand that each spectral component form an individual interference pattern. It is known from the experiment that the interference fringes are observed only if:

$$\Delta t \leq \frac{2\pi}{\Delta\omega} \tag{3.10}$$

The maximum time delay $\tau_c = \frac{2\pi}{\Delta\omega}$ and the corresponding path difference $l_c = \tau_c c = \frac{2\pi c}{\Delta\omega}$ are called coherence time and coherence length, respectively. Therefore temporal coherence is the measurement of how monochromatic the light is. An ideal light source would have an infinite coherence time.

Coherence length l_c can be seen as the distance in the direction of propagation of wave, where the amplitude and phase of the wave could be considered well defined and predictable. Therefore, within this distance there is a possibility for interference. Temporal coherence is sometimes called longitudinal coherence.

In other words, if the phase difference between the electric field of an electromagnetic wave at different times t and $t + \tau$ at a fixed position is fixed for every value of $0 < \tau \leq \tau_c$, the wave is partially coherent temporally. For a perfectly coherent beam, the coherence time is infinity and for completely incoherent light, $\tau = 0$.

Figure 3.2 shows an example of a partially coherent wave with coherence time τ_1 where the sinusoidal electric field experiences random phase change at
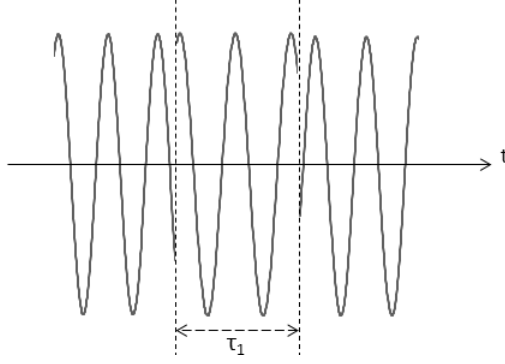
Figure 3.2: An example of a wave with finite coherence time τ_1
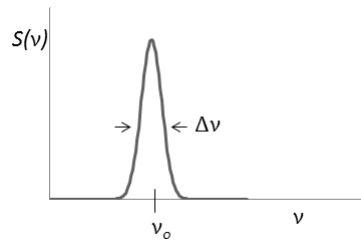
Figure 3.3: Spectral density and bandwidth of wave in figure 3.2

time intervals τ_1. By comparing this figure to the sinusoidal wave in figure 3.1, it is obvious that the latter can be represented by a sinusoidal function with exact frequency, while according to the Fourier transform principle the former can be represented as the sum of an infinite number of pure sinusoidal waves. According to the Wiener-Khinchin theorem [26], the spectral density $S(\nu)$ and autocorrelation function are Fourier transform pairs:

$$S(\nu) = \int_{-\infty}^{\infty} C(\tau)exp(-i2\pi\nu\tau)d\tau \qquad (3.11)$$

The width of $S(\nu)$ is the spectral width or line width $\Delta\nu$ equivalent to $\Delta\omega$. There are several definitions for spectral width but the most common one is the full width of the function $S(\nu)$ at half its maximum (FWHM). In figure 3.3 the spectral width is shown for the wave in figure 3.2 for a Gaussian frequency distribution. The exact relationship between τ_c and $\Delta\nu$ depends on the shape of $S(\nu)$, but what is important is that there is an inverse relationship

30

Figure 3.4: Finite (left) and infinite (right) coherence area

between them $\Delta\nu \sim \frac{1}{\tau_c}$. That means the longer the coherence time, the more monochromatic the wave. For example, sunlight has the bandwidth of $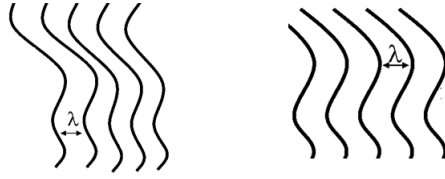\Delta\nu \approx 5 \times 10^{14}\,Hz$ and coherence time of only $2\,fs$, while even a broadband laser with $\Delta\nu \approx 1\,MHz$ has $1\,\mu s$ coherence time [32].

The coherence time provides a lower limit to the duration of a laser pulse. That means in the case that the entire spectrum of the pulse is due to the short duration of its envelope, the coherence time and pulse duration are equal [33].

3.4 Spatial Coherence

Spatial coherence is the cross-correlation of two points in space at all times as shown by equation (3.8). If all the points along the wave front are correlated, then the beam is spatially coherent, however if it is true for a specific area, the wave is only partially coherent. An example is shown in figure 3.4. It is also called transverse coherence because the phase difference of two points on a plane perpendicular to the direction of the propagation of beam is time independent. Spatial coherence can be related to the size of the source since for a source with a finite size, emission from each point is independent from the other. In case of the laser, although the laser medium has finite cross section, the light is the result of the stimulated emission of atoms or molecules and therefore the spatial coherence is high.

The temporal and spatial fluctuations of light are related since the complex wave function must satisfy wave equation which imposes conditions on the

mutual coherence function [26].

The degree of contrast of the interference fringes in Young experiment is a measure of spatial coherence. The more the light is spatially coherent, the smaller the divergence and the better the directionality.

3.5 Gaussian Correlation Function

The goal of this section is the development of a correlation function for a partially coherent beam i.e. the solution to the wave equation in paraxial approximation. Then two limiting cases for the correlation function are considered. Consider the electric field of an electromagnetic wave with frequency ω which its amplitude dependent on position and time. If for convenience, the direction of propagation is assumed along the z-axis, the electric field is:

$$\mathbf{E}(\mathbf{r}, t) = \mathbf{E_0}(\mathbf{r}, t)e^{ikz - i\omega t} \tag{3.12}$$

which satisfies wave equation:

$$\nabla^2 \mathbf{E} - \frac{1}{c^2}\frac{\partial^2 \mathbf{E}}{\partial t^2} = 0 \tag{3.13}$$

Substitution into wave equation (3.13) requires taking first and second order time derivatives:

$$\frac{\partial \mathbf{E}}{\partial t} = (\frac{\partial \mathbf{E_0}}{\partial t} - i\omega \mathbf{E})e^{ikz - i\omega t} \tag{3.14}$$

$$\frac{\partial^2 \mathbf{E}}{\partial t^2} = (\frac{\partial^2 \mathbf{E_0}}{\partial t^2} - 2i\omega \frac{\partial \mathbf{E_0}}{\partial t} - \omega^2 \mathbf{E_0})e^{ikz - i\omega t} \tag{3.15}$$

where the exponential part $e^{ikz - i\omega t}$ can be dropped. Splitting the Laplacian into transverse and parallel components ($\nabla^2 = \nabla_\perp^2 + \frac{\partial^2}{\partial z^2}$), we have:

$$\frac{\partial^2 \mathbf{E}}{\partial z^2} = \frac{\partial^2 \mathbf{E_0}}{\partial z^2} + 2ik\frac{\partial \mathbf{E_0}}{\partial z} - k^2 \mathbf{E_0} \qquad (3.16)$$

and using $\nabla_\perp^2 = \frac{\partial^2}{\partial r_\perp^2} + \frac{1}{r_\perp}\frac{\partial}{\partial r_\perp}$, we have:

$$\nabla_\perp^2 \mathbf{E_0} + \frac{\partial^2 \mathbf{E_0}}{\partial z^2} - 2ik\frac{\partial \mathbf{E_0}}{\partial z} - k^2 \mathbf{E_0} - \frac{1}{c^2}\left(\frac{\partial^2 \mathbf{E_0}}{\partial t^2} - 2i\omega\frac{\partial \mathbf{E_0}}{\partial t} - \omega^2 \mathbf{E_0}\right) = 0 \quad (3.17)$$

Now if we use the dispersion relation in vacuum $\omega = kc$:

$$\nabla_\perp^2 \mathbf{E_0} + \frac{\partial^2 \mathbf{E_0}}{\partial z^2} - 2ik\frac{\partial \mathbf{E_0}}{\partial z} - \frac{1}{c^2}\left(\frac{\partial^2 \mathbf{E_0}}{\partial t^2} - 2i\omega\frac{\partial \mathbf{E_0}}{\partial t}\right) = 0 \qquad (3.18)$$

Paraxial wave approximation means:

1. Variation of the field along the direction of propagation is small over a distance comparable to the wavelength i.e. $|\frac{\partial^2 \mathbf{E_0}}{\partial z^2}| \ll 2k|\frac{\partial \mathbf{E_0}}{\partial z}|$

2. Axial variation will be small compared to variation perpendicular to this direction i.e. $|\frac{\partial^2 \mathbf{E_0}}{\partial z^2}| \ll \nabla_\perp^2 \mathbf{E_0}$

We also assume that the variation of field over a time comparable to period of the field is small i.e. $|\frac{\partial^2 \mathbf{E_0}}{\partial t^2}| \ll \omega|\frac{\partial \mathbf{E_0}}{\partial t}|$

These assumptions mean we can drop second order derivatives $\frac{\partial^2 \mathbf{E_0}}{\partial z^2}$ and $\frac{\partial^2 \mathbf{E_0}}{\partial t^2}$ in equation (3.18) leading to:

$$\nabla_\perp^2 \mathbf{E_0} - 2ik\frac{\partial \mathbf{E_0}}{\partial z} - \frac{2i\omega}{c^2}\frac{\partial \mathbf{E_0}}{\partial t} = 0 \qquad (3.19)$$

Now we can use the fact that mutual coherence function also satisfies the wave equation. One can see that from multiplying equation (3.19) by $\mathbf{E_0^*}(\mathbf{r}', t')$ and taking the ensemble average, which gives the correlation function:

$$C_{EE^*}(\mathbf{r} - \mathbf{r}', t - t') = \langle \mathbf{E_0}(\mathbf{r}, t)\,\mathbf{E_0^*}(\mathbf{r}', t')\rangle \qquad (3.20)$$

The proposed solution is the Gaussian Correlation function from reference [34] which approximates optically smoothed (partially coherent) laser beam:

$$C_{EE^*}^G(\mathbf{r} - \mathbf{r}', t - t') = \frac{\epsilon_0^2}{1 + i(z - z')/L_R} \cdot$$
$$exp(-\frac{(\mathbf{r}_\perp - \mathbf{r}'_\perp)^2}{2a_0^2(1 + i(z - z')/L_R)} - \frac{(t - t' - (z - z')/v_g)^2}{2\tau_0^2}) \tag{3.21}$$

The coherence of the beam depends on two parameters: τ_0 the probe correlation time and a_0 the minimum radius of hot spot (beam waist) or transverse correlation length which is related to Rayleigh length L_R or longitudinal correlation length as $L_R = k_0 a_0^2$. The wave group velocity v_g satisfies $v_g = k_0 c^2/\omega_0 \approx c$ where k_0 and ω_0 are the wave number and angular frequency of the wave, respectively and ϵ_0 is the constant part of the electric field amplitude. Now by applying Fourier transformation

$$C_{EE^*}^G(\mathbf{k}, \omega) = \int_{-\infty}^{+\infty} d(t - t') e^{i\omega(t-t')} \int d^3(\mathbf{r} - \mathbf{r}') e^{-i\mathbf{k}\cdot(\mathbf{r}-\mathbf{r}')} C_{EE^*}^G(\mathbf{r} - \mathbf{r}', t - t') \tag{3.22}$$

to equation (3.21), the spectral Gaussian correlation function is found:

$$C_{EE^*}^G(\mathbf{k}, \omega) = (2\pi)^{5/2} \epsilon_0^2 a_0^2 \tau_0 \, \delta(k_z - \frac{\omega}{v_g} + \frac{a_0^2 k_\perp^2}{2L_R}) \, exp(-\frac{1}{2}\omega^2\tau_0^2 - \frac{1}{2}a_0^2 k_\perp^2) \tag{3.23}$$

Chapter 4

Dressed Test Particle Method and Definition of Plasma Form Factor

In this chapter, we will find the dynamic from factor $S(\mathbf{k}, \omega)$ in general form for an unmagnetized, stationary and homogeneous plasma by applying dressed test particle method to a plasma near equilibrium. Then, this function is analyzed for a specific plasma with Maxwellian distribution function.

4.1 Klimontovich and Vlasov Equations

For a particle moving along trajectory $\mathbf{r_i}(t)$ with velocity $\mathbf{v_i}(t)$, the trajectory in six dimensional phase space (of position $\mathbf{r}$ and velocity $\mathbf{v}$) can be described in terms of microscopic density:

$$\delta(\mathbf{r} - \mathbf{r_i})\, \delta(\mathbf{v} - \mathbf{v_i}) \tag{4.1}$$

Therefore, for a plasma with N^α number of particle of species α, where $\alpha = e, i$

for electrons and ions respectively; the microscopic density is:

$$\aleph^{\alpha}(\mathbf{r}, \mathbf{v}, t) = \sum_{i=1}^{N^{\alpha}} \delta\big(\mathbf{r} - \mathbf{r_i}(t)\big)\, \delta\big(\mathbf{v} - \mathbf{v_i}(t)\big) \tag{4.2}$$

Using chain rule, partial time derivative of $\aleph^{\alpha}$ gives:

$$\frac{\partial \aleph^{\alpha}}{\partial t} = \sum_{i=1}^{N^{\alpha}} \Big(\frac{\partial \mathbf{r_i}}{\partial t} \cdot \nabla_{r_i} + \frac{\partial \mathbf{v_i}}{\partial t} \cdot \nabla_{v_i}\Big)\, \delta(\mathbf{v} - \mathbf{v_i})\, \delta(\mathbf{v} - \mathbf{v_i}) \tag{4.3}$$

Using the identities for a function f:

$$\frac{\partial\, f(a - b)}{\partial\, a} = -\frac{\partial\, f(a - b)}{\partial\, b} \tag{4.4}$$

and

$$f(a)\, \delta(a - b) = f(b)\, \delta(a - b)\,. \tag{4.5}$$

we have:

$$\frac{\partial \aleph^{\alpha}}{\partial t} = -\big(\mathbf{v} \cdot \nabla_r + \mathbf{a} \cdot \nabla_v\big) \sum_{i=1}^{N^{\alpha}} \delta(\mathbf{r} - \mathbf{r_i})\, \delta(\mathbf{v} - \mathbf{v_i})\,, \tag{4.6}$$

where due to delta functions, $\mathbf{v}_i = \frac{\partial \mathbf{r}_i}{\partial t}$ and $\mathbf{a}_i = \frac{\partial \mathbf{v}_i}{\partial t}$ are velocity and acceleration respectively. Using equations (4.2) and (4.6) and definition of total derivative leads to:

$$\frac{d \aleph^{\alpha}}{dt} = \frac{\partial \aleph^{\alpha}}{\partial t} + \mathbf{v} \cdot \nabla_r \aleph^{\alpha} + \mathbf{a} \cdot \nabla_v \aleph^{\alpha} = 0 \tag{4.7}$$

meaning that the Klimontovich distribution function satisfies continuity equation.

Neglecting gravity, the only force acting on a particle with charge q_{α} and mass m_{α}, is the Lorentz force from microscopic electric and magnetic fields $\mathbf{E}(\mathbf{r}, t)$ and $\mathbf{B}(\mathbf{r}, t)$, leading to acceleration $\mathbf{a} = \frac{q_{\alpha}}{m_{\alpha}}(\mathbf{E} + \frac{1}{c}\mathbf{v} \times \mathbf{B})$. The equation (4.7) is known as the Klimontovich equation for the microscopic density $\aleph^{\alpha}$ from equation (4.2) as:

36

$$\frac{\partial \aleph^\alpha}{\partial t} + \mathbf{v} \cdot \nabla_r \aleph^\alpha + \frac{q_\alpha}{m_\alpha} \left(\mathbf{E} + \frac{1}{c} \mathbf{v} \times \mathbf{B} \right) \cdot \nabla_v \aleph^\alpha = 0 \tag{4.8}$$

Equation (4.8) provides the exact microscopic description of a plasma in a $6N$ dimensional phase space. Due to the discreteness of particles, $\aleph^\alpha$ is not smooth. Also, since it is a partial differential equation, in order to have exact solutions, initial and boundary conditions should be known. This and the fact that the number of equations is exteremely large, makes equation (4.8) of no practical importance [35].

The physical measurements correspond to statistical averages of microscopic densities. Therefore, by introducing an appropriate statistical averaging, equation (4.8) leads to equations for smooth functions. The particle distribution function $f_\alpha(\mathbf{v}, \mathbf{r}, t)$ is in fact the ensemble average of microscopic density:

$$\langle \aleph^\alpha \rangle = f_\alpha(\mathbf{v}, \mathbf{r}, t) \tag{4.9}$$

Using (4.9), $\aleph^\alpha$ can be split into averaged and fluctuating parts:

$$\aleph^\alpha(\mathbf{v}, \mathbf{r}, t) = f_\alpha(\mathbf{v}, \mathbf{r}, t) + \delta f_\alpha(\mathbf{v}, \mathbf{r}, t) \tag{4.10}$$

where $\langle \delta f_\alpha \rangle = 0$.

The fields also consist of two separate parts: the first part being $\mathbf{E}(\mathbf{r}, t)$ and $\mathbf{B}(\mathbf{r}, t)$ which are contributions from external sources (e.g. electromagnetic waves propagating in a plasma described by $f_\alpha(\mathbf{v}, \mathbf{r}, t)$) and charge current densities due to inhomogeneity of $f_\alpha(\mathbf{v}, \mathbf{r}, t)$. The second part, $\delta \mathbf{E}$ and $\delta \mathbf{B}$, corresponds to fluctuations due to particle discreteness:

$$\mathscr{E}(\mathbf{r}, t) = \mathbf{E}(\mathbf{r}, t) + \delta \mathbf{E} , \tag{4.11}$$

$$\mathscr{B}(\mathbf{r}, t) = \mathbf{B}(\mathbf{r}, t) + \delta \mathbf{B} . \tag{4.12}$$

Now equations (4.10), (4.11) and (4.12) can be substituted into equation (4.8). Taking ensemble average and using the fact that $\langle \delta f_\alpha \rangle = \langle \delta \mathbf{E} \rangle = \langle \delta \mathbf{B} \rangle = 0$, then leads to kinetic equation for smooth one particle distribution function:

$$\frac{\partial f_\alpha}{\partial t} + \mathbf{v} \cdot \nabla_r f_\alpha + \frac{q_\alpha}{m_\alpha} (\mathbf{E} + \frac{1}{c} \mathbf{v} \times \mathbf{B}) \cdot \nabla_v f_\alpha = -\frac{q_\alpha}{m_\alpha} \left\langle \nabla_v \delta f_\alpha \cdot (\delta \mathbf{E} + \frac{1}{c} \mathbf{v} \times \delta \mathbf{B}) \right\rangle \quad (4.13)$$

The left hand side of equation (4.13) describes the evolution of one particle distribution function f_α, while the right hand side describes correlations of fluctuations, including particle collisions [36].

Assuming that perturbation are small, we can ignore second order terms. This means that the right hand side vanishes and plasma is collisionless.

$$\frac{\partial f_\alpha}{\partial t} + \mathbf{v} \cdot \nabla_r f_\alpha + \frac{q_\alpha}{m_\alpha} (\mathbf{E} + \frac{1}{c} \mathbf{v} \times \mathbf{B}) \cdot \nabla_v f_\alpha = 0 \quad (4.14)$$

The Vlasov equation (4.14) togheter with Maxwell equations constitute a kinetic model of collisionless plasma. Since distrbution function depends on electromagnetic fields, the last term on the left side of equation (4.14) makes it nonlinear with respect to those fields [35].

Equations (4.7) and (4.14) seem similar, but are fundamentally different, since Klimontovich equations is the description at microscopic level containing discreteness and individuality of particle, while the Vlasov equation is macroscopic and discreteness is lost due to averaging process [37].

Plasmas that have evolved toward stationary and homogeneous state. characterized by $f^\alpha(\mathbf{v})$, can be wall approximated by the linearized Vlasov equation:

$$\frac{\partial \, \delta f^\alpha}{\partial t} + \mathbf{v} \cdot \nabla_r \delta f^\alpha + \frac{q_\alpha}{m_\alpha} \delta \mathbf{E} \cdot \nabla_v f^\alpha = 0 \quad (4.15)$$

where $f_\alpha(\mathbf{v}, \mathbf{r}, t) = f^\alpha(\mathbf{v}) + \delta f^\alpha(\mathbf{v}, \mathbf{r}, t)$, and $\delta f^\alpha \ll f^\alpha$. The small deviations of the distribution function δf^α and corresponding field perturbations $\delta \mathbf{E}$, are continuous functions. They will describe polarization effects in the Vlasov

plasma in response to discrete test particle in the dressed test particle method, that is discussed in the next section.

One of the most important theories of plasma kinetics near equilibrium is the dressed particle method, which will be discussed in the next section.

4.2 Dressed Test Particle Method

The assumption of plasma being near equilibrium means that fluctuations should be small and therefore, linear response is assumed. This assumption was already made to derive equation (4.15).

In dressed test particle approach, each particle in plasma is treated as a test particle. To do so, we isolate one particle and assume that it is moving with velocity $\mathbf{v_i}$ along a straight trajectory,

$$\mathbf{r_i}(t) = \mathbf{r_i'} + \mathbf{v_i}t \, , \tag{4.16}$$

where $\mathbf{r_i'}$ is the initial condition. For particles of type α, the perturbation in phase space due to their movement will be:

$$\delta f_t^\alpha(\mathbf{r}, \mathbf{v}, t) = \sum_{i=1}^{N^\alpha} \delta(\mathbf{r} - \mathbf{r_i}(t)) \, \delta(\mathbf{v} - \mathbf{v_i}) \tag{4.17}$$

In response of this perturbation, the medium becomes polarized. Particles of type α participate in screening process of different species; particles of α type and non α type. We can also distinguish two parts in fluctuations: first the initial perturbation and second the screening as the response to that. By assuming all particles in plasma as test particles, we can write Gauss' law as:

$$\nabla \cdot \delta \mathbf{E} = 4\pi \sum_\beta \left(\delta n_t^\beta q_\beta + q_\beta n_\beta \int d^3v \, \delta f^\beta \right) \tag{4.18}$$

where $\delta n_t^\beta = \int d^3v \, \delta f_t^\beta$ are the density fluctuations corresponding to initial

perturbation and the second term corresponding to screening process. Since all particles take part in screening of all other particles, we split fluctuations in phase space for α particles to two parts:

$$\delta f^\alpha = \delta f_1^\alpha + \delta f_2^\alpha \tag{4.19}$$

The first part is the perturbation of α particle density distribution that describes polarization of the plasma in response to test particle of type α. The second part is related to the polarization of α type particles in response to test particles of type $\beta(\neq \alpha)$. Linearized Vlasov equation for α species, equation (4.15) can be split into two parts:

$$\frac{\partial \delta f_1^\alpha}{\partial t} + \mathbf{v} \cdot \nabla_r \delta f_1^\alpha + \frac{q_\alpha}{m_\alpha} \, \delta \mathbf{E_1} \cdot \nabla_v f^\alpha = 0 \tag{4.20}$$

$$\frac{\partial \delta f_2^\alpha}{\partial t} + \mathbf{v} \cdot \nabla_r \delta f_2^\alpha + \frac{q_\alpha}{m_\alpha} \, \delta \mathbf{E_2} \cdot \nabla_v f^\alpha = 0 \tag{4.21}$$

where $\delta \mathbf{E} = \delta \mathbf{E_1} + \delta \mathbf{E_2}$ are associated field fluctuations. For these field fluctuations, we can write Gauss' law consistent with the separation that we made. Now separating α type, Gauss' equations for two parts can be written as:

$$\nabla \cdot \delta \mathbf{E_1} = 4\pi \left(\delta n_t^\alpha + \sum_\beta q_\beta n_\beta \int d^3v \, \delta f_1^\beta \right) \tag{4.22}$$

$$\nabla \cdot \delta \mathbf{E_2} = 4\pi \left(\sum_{\beta \neq \alpha} \delta n_t^\beta + \sum_\beta q_\beta n_\beta \int d^3v \, \delta f_2^\beta \right) \tag{4.23}$$

To solve equations (4.22) and (4.23), we use Fourier transformation in space and time as:

$$\delta f^\alpha(\mathbf{k}, \mathbf{v}, \omega) = \int_{-\infty}^{+\infty} dt \, e^{i\omega t} \int_{-\infty}^{+\infty} d^3r \, e^{-i\mathbf{k}\cdot\mathbf{r}} \, \delta f^\alpha(\mathbf{r}, \mathbf{v}, t) \tag{4.24}$$

Applying Fourier transformation to equation (4.20) and noting that $\delta \mathbf{E_1} =$

$-\nabla\Phi_1$, we have:

$$\left(\mathbf{k}\cdot\mathbf{v} - \omega\right)\delta f_1^\alpha = \frac{q_\alpha}{m_\alpha}\,\Phi_1\left(\mathbf{k}\cdot\nabla_v f^\alpha\right) \tag{4.25}$$

Solving for δf_1^α:

$$\delta f_1^\alpha = -\frac{q_\alpha}{m_\alpha}\frac{1}{\omega - \mathbf{k}\cdot\mathbf{v} + i\eta}\,\mathbf{k}\cdot\nabla_v f^\alpha\,\Phi_1(\mathbf{k},\omega) \tag{4.26}$$

where imaginary part with small η in denominator is used to avoid singularity at $\omega = \mathbf{k}\cdot\mathbf{v}$. The plasma susceptibility $\chi^\alpha(\mathbf{k},\omega)$ is defined as:

$$\chi^\alpha(\mathbf{k},\omega) = \frac{\omega_{p\alpha}^2}{k^2}\int d^3v\,\frac{1}{\omega - \mathbf{k}\cdot\mathbf{v} + i\eta}\,\mathbf{k}\cdot\nabla_v f^\alpha \tag{4.27}$$

where $\omega_{p\alpha}^2 = \frac{4\pi q_\alpha^2 n_\alpha}{m_\alpha}$ is plasma frequency. Multiplying equation (4.26) by $q_\alpha n_\alpha$ and integration over velocity, we can write:

$$q_\alpha\,\delta n_1^\alpha = n_\alpha q_\alpha\int d^3v\,\delta f_1^\alpha = -\frac{k^2}{4\pi}\,\chi^\alpha(\mathbf{k},\omega)\,\Phi_1(\mathbf{k},\omega) \tag{4.28}$$

Using this equation to find potential, we apply Fourier transformation to equation (4.22):

$$k^2\,\Phi_1(\mathbf{k},\omega) = 4\pi\Big(q_\alpha\,\delta n_t^\alpha - \sum_\beta \frac{k^2}{4\pi}\,\chi^\beta\,\Phi_1(\mathbf{k},\omega)\Big) \tag{4.29}$$

to find:

$$\Phi_1(\mathbf{k},\omega) = \frac{4\pi q_\alpha\,\delta n_t^\alpha}{k^2\big(1 + \sum_\beta \chi^\beta\big)} \tag{4.30}$$

Substitution of potential from equation (4.28) and using the relationship between dielectric response function and susceptibility $\epsilon(\mathbf{k},\omega) = 1 + \sum_\beta \chi^\beta(\mathbf{k},\omega)$ we find:

$$\delta n_1^\alpha = -\frac{\chi^\alpha(\mathbf{k},\omega)}{\epsilon(\mathbf{k},\omega)}\,\delta n_t^\alpha \tag{4.31}$$

Finding δn_2^α follows similar steps, using equations (4.21) and (4.23) instead to find:

$$\delta n_2^\alpha = -\frac{k^2}{4\pi} \chi^\alpha(\mathbf{k}, \omega) \, \Phi_2(\mathbf{k}, \omega) \tag{4.32}$$

and:

$$\Phi_2(\mathbf{k}, \omega) = \frac{4\pi q_\alpha \sum_{\beta \neq \alpha} q_\beta \, \delta n_t^\beta}{k^2 \epsilon(\mathbf{k}, \omega)} \tag{4.33}$$

resulting to:

$$\delta n_2^\alpha = -\frac{\chi^\alpha(\mathbf{k}, \omega)}{\epsilon(\mathbf{k}, \omega)} \sum_{\beta \neq \alpha} \frac{q_\beta}{q_\alpha} \, \delta n_t^\beta \tag{4.34}$$

Total fluctuations are sum of all fluctuations $\delta n^\alpha = \delta n_t^\alpha + \delta n_1^\alpha + \delta n_2^\alpha$, leading to:

$$\delta n^\alpha = \left(1 - \frac{\chi^\alpha(\mathbf{k}, \omega)}{\epsilon(\mathbf{k}, \omega)}\right) \delta n_t^\alpha - \frac{\chi^\alpha(\mathbf{k}, \omega)}{\epsilon(\mathbf{k}, \omega)} \sum_{\beta \neq \alpha} \frac{q_\beta}{q_\alpha} \delta n_t^\beta \tag{4.35}$$

Our goal is to find electron density fluctuation correlation function:

$$
\begin{aligned}
\langle |\delta n^e(\mathbf{k}, \omega))|^2 \rangle &= \left| 1 - \frac{\chi^e(\mathbf{k}, \omega)}{\epsilon(\mathbf{k}, \omega)} \right|^2 \langle |\delta n_t^e(\mathbf{k}, \omega)|^2 \rangle \\
&+ \left| \frac{\chi^e(\mathbf{k}, \omega)}{\epsilon(\mathbf{k}, \omega)} \right|^2 \sum_{\beta \neq \alpha} Z_\beta^2 \langle |\delta n_t^\beta(\mathbf{k}, \omega)|^2 \rangle
\end{aligned}
\tag{4.36}
$$

By calculating $\langle \delta f_t^\alpha(\mathbf{r}, \mathbf{v}, t) \delta f_t^\beta(\mathbf{r}', \mathbf{v}', t') \rangle$ and applying Fourier transformation, it is found:

$$\langle |\delta n_t^\alpha(\mathbf{k}, \omega))|^2 \rangle = 2\pi \int d^3 v \, \delta(\omega - \mathbf{k} \cdot \mathbf{v}) \, f^\alpha(\mathbf{v}) = \frac{2\pi}{k} \, n_{0\alpha} \, \overline{f}^\alpha(v = \omega/k) \tag{4.37}$$

as the test particles are uncorrelated except for autocorrelations of the same particle at different positions and times. Therefore, by substitution in equation (4.38):

$$S(\mathbf{k}, \omega) = \frac{\langle |\delta n^e(\mathbf{k}, \omega))|^2 \rangle}{n_{0e}}$$

$$= \frac{2\pi}{k} \left| 1 - \frac{\chi^e(\mathbf{k}, \omega)}{\epsilon(\mathbf{k}, \omega)} \right|^2 \overline{f}^e(v = \omega/k) \tag{4.38}$$

$$+ \frac{2\pi}{k} \left| \frac{\chi^e(\mathbf{k}, \omega)}{\epsilon(\mathbf{k}, \omega)} \right|^2 \sum_{\beta \neq \alpha} Z_\beta^2 \, \overline{f}^\beta(v = \omega/k)$$

Equation (4.38) defines dynamic form factor, that is an important part of the Thomson Scattering cross section in equation (2.51).

4.3 Maxwellian Plasma and Plasma Dispersion Function

When plasma is in thermal equilibrium and obeys the classical statistics, the velocity distribution is given by the Maxwellian:

$$f_\alpha^M(v) = \left(\frac{m_\alpha}{2\pi T_\alpha} \right)^{3/2} exp\left(-\frac{mv^2}{2T_\alpha} \right) \tag{4.39}$$

furthermore, x-axis is chosen as the direction of the wave vector $\mathbf{k} = k\,\widehat{\mathbf{x}}$. Starting from dielectric response function:

$$\chi^\alpha(\mathbf{k}, \omega) = \frac{\omega_{p\alpha}^2}{k^2} \int d^3v \, \frac{1}{\omega - \mathbf{k} \cdot \mathbf{v} + i\eta} \, \mathbf{k} \cdot \nabla_v f_\alpha^M \tag{4.40}$$

we have:

$$\chi^\alpha(\mathbf{k}, \omega) = \frac{k_D^2}{k^2} \sqrt{\frac{m_\alpha}{2\pi T_\alpha}} \int_{-\infty}^{\infty} dv_x \, \frac{-kv_x}{\omega - kv_x + i\eta} \, exp\left(-\frac{m_\alpha v_x^2}{2T_\alpha} \right) \tag{4.41}$$

Introducing parameters $w = v_x/v_{th}^\alpha$ and $\xi_\alpha = \omega/kv_{th}^\alpha$, where $v_{th}^\alpha = \sqrt{\frac{T_\alpha}{m_\alpha}}$ is the mean thermal speed of the species α, equation (4.41) can be modified as:

$$\chi^{\alpha}(\mathbf{k}, \xi) = \frac{k_D^2}{k^2} \frac{1}{\sqrt{2\pi}} \int_{-\infty}^{\infty} dw \, \frac{-w}{\xi - w + i\eta} \, e^{-w^2/2} \tag{4.42}$$

This is a well defined function in the upper half of the complex plane ($\eta > 0$). Therefore, the contour of w integration in the complex plane can be changed in such a way that ξ remains above the path [37]. The W function defined as:

$$W(\xi) = \frac{1}{\sqrt{2\pi}} \int_c dw \, \frac{w}{\xi - w} \, e^{-w^2/2} \tag{4.43}$$

satisfies differential equation:

$$\frac{dW}{d\xi} = \left(\frac{1}{\xi} - \xi\right) W - \frac{1}{\xi} \tag{4.44}$$

with boundary condition $W(0) = 1$. $W(\xi)$ is related to the plasma dispersion function $Z(x)$ as:

$$W(x) = 1 + \frac{x}{\sqrt{2}} \, Z(\frac{x}{\sqrt{2}}) = -Z'(\frac{x}{\sqrt{2}}) \, /2 \tag{4.45}$$

where:

$$Z(x) \equiv \frac{1}{\sqrt{\pi}} \int_{-\infty}^{+\infty} dt \, \frac{e^{-t^2}}{x - t} \tag{4.46}$$

which satisfies:

$$Z'(x) = \frac{d \, Z(x)}{dx} = -2\big(1 + xZ(x)\big) \tag{4.47}$$

Solving equation (4.44) or evaluating integral(4.46) and using (4.45) are equivalent. To solve either, the following identity for real variable x should be substituted in respective equations:

$$\frac{1}{x - t} = i \int_0^{\infty} dy \, e^{-i(x-t)y} \tag{4.48}$$

Changing the order of integration and noting that $\int_0^{\infty} dy \, e^{-y^2} = \sqrt{\pi}/2$, leads

44

to:

$$W(\xi) = 1 - \xi\, e^{-\xi^2/2} \int_0^\xi dy\, e^{-y^2} + i\,\sqrt{\frac{\pi}{2}}\, \xi\, e^{-\xi^2/2} \tag{4.49}$$

and

$$Z(x) = i\,\sqrt{\pi}\, e^{-x^2} - 2\,e^{-x^2} \int_0^x e^{t^2} dt \tag{4.50}$$

Using the error function (erf), and imaginary error function ($erfi$) defined as:

$$erf(y) = \frac{2}{\sqrt{\pi}} \int_0^y e^{-t^2} dt \tag{4.51}$$

and

$$erfi(y) = -i\,erf(ix) = \frac{2}{\sqrt{\pi}} \int_0^y e^{t^2} dt \tag{4.52}$$

equations (4.49) and (4.50) can be expressed as:

$$W(\xi) = 1 - \frac{\sqrt{\pi}}{2}\, \xi\, e^{-\xi^2/2} \left(erfi(\xi) - i\sqrt{2}\right) \tag{4.53}$$

$$Z(x) = i\sqrt{\pi}e^{-x^2}\left(1 + erfi(x)\right) \tag{4.54}$$

Substitution of equation (4.43) into equation (4.42) and using equation (4.53) for electrons and ions, susceptibilities in term of real ($\Re W$) and imaginary ($\Im W$) part of W are respectively:

$$\chi^e(\mathbf{k},\omega) = \alpha^2 \left(\Re W(x_e) + i\,\Im W(x_e)\right) \tag{4.55}$$

and

$$\chi^i(\mathbf{k},\omega) = \alpha^2\,\frac{ZT_e}{T_i} \left(\Re W(x_i) + i\,\Im W(x_i)\right) \tag{4.56}$$

where T_e and T_i are electron and ion temperatures, Z is the atomic number of ion, $x_\alpha = \frac{\omega}{\sqrt{2}kv_{th}^\alpha}$ and $W(x)$ is defined as:
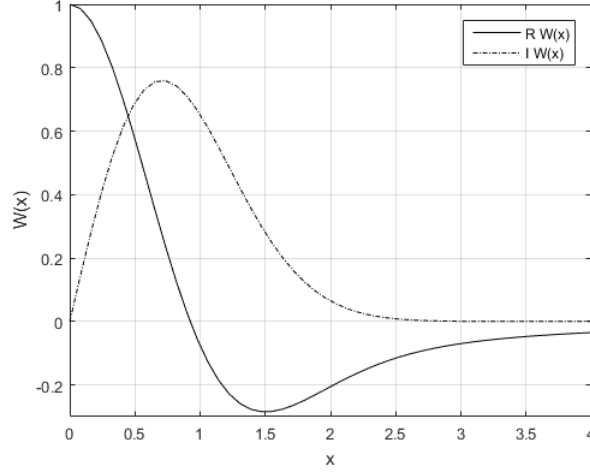
Figure 4.1: Real and imaginary parts of W as a function of x

$$W(x) = 1 - 2x\, e^{-x^2} \int_0^x e^{-t^2} dt + i\, \sqrt{\pi} x\, e^{-x^2} \tag{4.57}$$

In figure 4.1, the real and imaginary parts of equation (4.57) are shown.

Now, the form factor $S(\mathbf{k}, \omega)$ can be written as [10]:

$$S(\mathbf{k}, \omega) = \frac{2\sqrt{\pi}}{k v_{th}^e} \left(\frac{A_e + A_i}{|\epsilon|^2} \right) \tag{4.58}$$

where:

$$A_e = e^{-x_e^2} \left\{ \left(1 + \alpha^2\, \frac{ZT_e}{T_i}\, \Re W(x_i) \right)^2 + \left(\alpha^2\, \frac{ZT_e}{T_i}\, \Im W(x_i) \right)^2 \right\} \tag{4.59}$$

and

$$A_i = Z\, \sqrt{\frac{m_i\, T_e}{m_e\, T_i}}\, e^{-x_i^2} \left\{ \left(\alpha^2\, \Re W(x_e) \right)^2 + \left(\alpha^2\, \Im W(x_e) \right)^2 \right\} \tag{4.60}$$
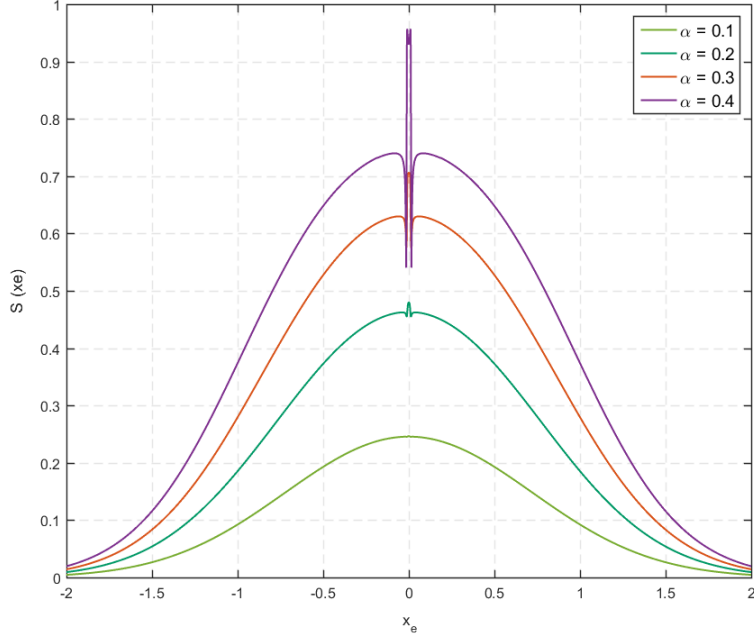
are electron and ion components respectively and:

Figure 4.2: Effect of variation of α on $S(x_e)$

$$
\begin{aligned}
|\epsilon|^2 &= \left\{ 1 + \alpha^2 \left(\Re W(x_e) + \frac{ZT_e}{T_i} \Re W(x_i) \right) \right\}^2 \\
&+ \left\{ \alpha^2 \left(\Im W(x_e) + \frac{ZT_e}{T_i} \Im W(x_i) \right) \right\}^2
\end{aligned}
\tag{4.61}
$$

4.4   Electron Plasma and Ion-acoustic Waves

Two parameters that determine whether resonances happen in $S(\mathbf{k}, \omega)$ are $\alpha = 1/k\lambda_D$ and ZT_e/T_i.

Using equation (4.58), collective and non-collective scattering regimes can be distinguished. As discussed in section 2.2, in non-collective scattering $\alpha \ll 1$. Applying the limit $\alpha \to 0$ to equations (4.59), (4.60) and (4.61) results in $A_e \to e^{-x_e^2}$, $A_i \to 0$ and $|\epsilon|^2 \to 1$ respectively. Therefore, $S(\mathbf{k}, \omega) \to \frac{\sqrt{2\pi}}{kv_{th}^e} e^{-x_e^2}$ which is a Gaussian function representing electron thermal motion.

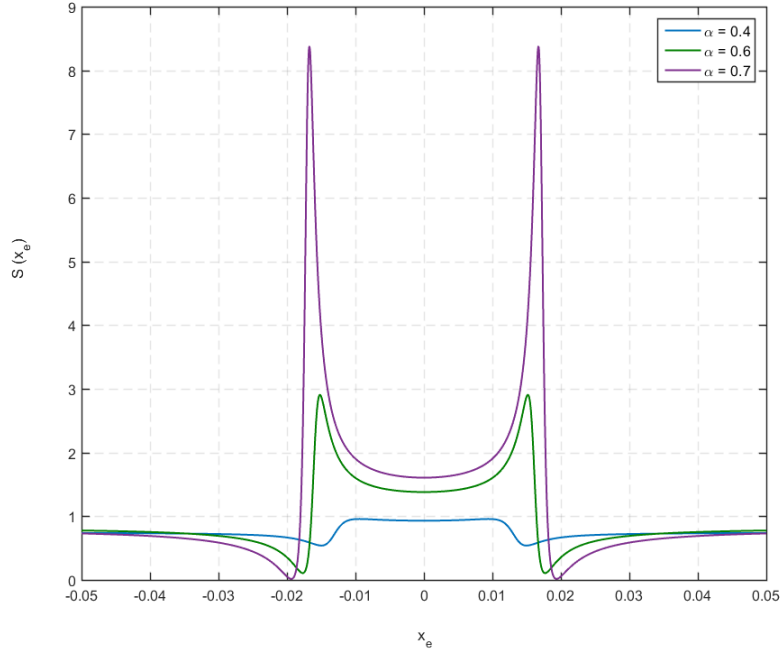As already discussed in the derivation of form factor in section 2.2, $A_e =$

47

Figure 4.3: Effect of variation of $\alpha < 1$ on $S(x_e)$ and ion-acoustic waves

$e^{-x_e^2}$ is only due to free electrons. This, in fact means that there is no collective response and the scattering is from individual electrons. On the other hand, $\alpha \geq 1$ implies that collective effects are important. As seen in figure 4.2, increase in α results in the appearance of resonances. Figures 4.2 to 4.5 are all plotted for scattering angle $\theta = 60°$, , for $T_e/T_i = 5$ and $^4_2He^{2+}$ ($Z = 2$ and $A = 4$) ions by varying α.

Figure 4.3 shows the resonances due to ion-acoustic fluctuations and figure 4.4 shows that as the result of increase in α, ion-acoustic waves become more prominent. The same effect is seen in Langmuir fluctuations in figure 4.5.

For $ZT_e/T_i < 1$ the scattering is primarily due to the electrons screening ions and therefore reflects ion velocity distribution. As seen in figure 4.6, which is plotted for $\alpha = 4$, ion-acoustic components become more marked as ZT_e/T_i increases.

For high frequencies $x_i \gg 1$, the ion component is negligible. To find resonance frequencies, roots of the real part of dielectric function must be
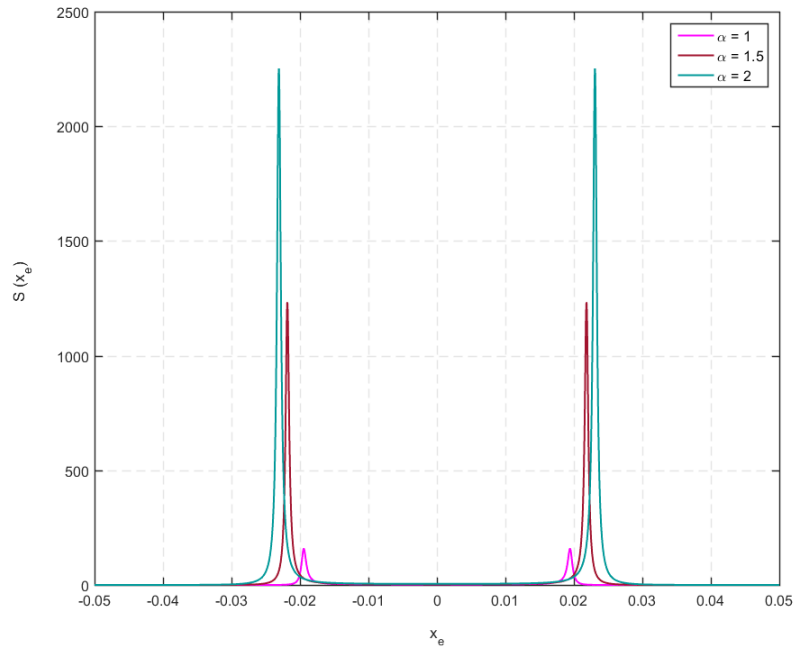
Figure 4.4: Effect of variation of $\alpha \geq 1$ on $S(x_e)$ ion-acoustic waves
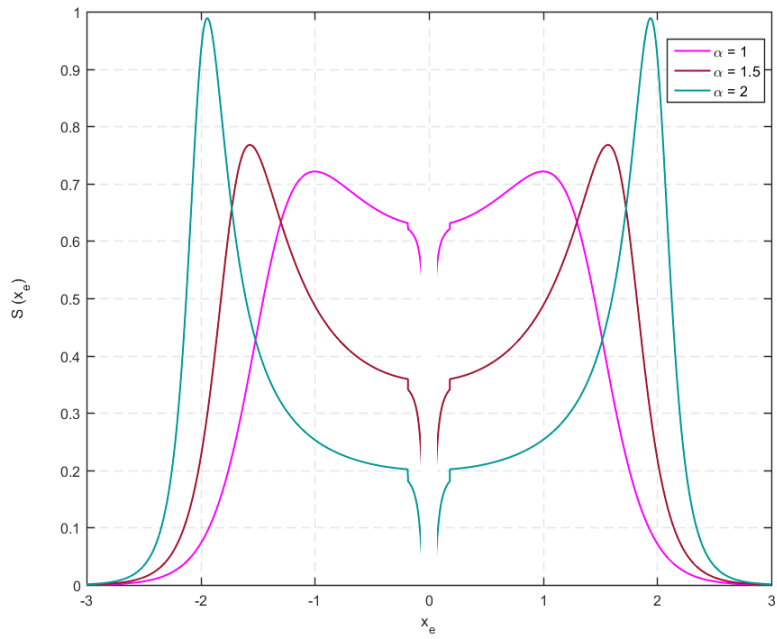

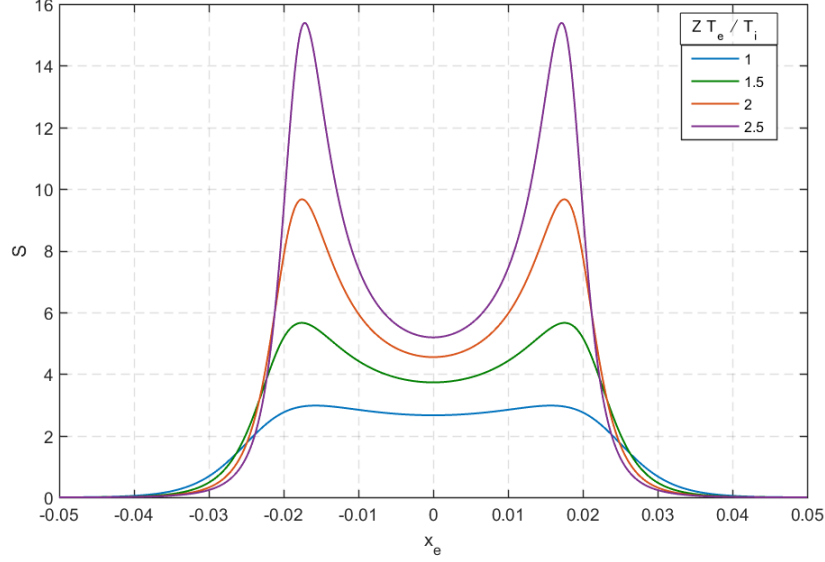Figure 4.5: Effect of variation of $\alpha \geq 1$ on $S(x_e)$ for Langmuir waves

49

Figure 4.6: Effect of variation of $Z\,T_e/T_i$ on $S(x_e)$ for $\alpha = 4$

found. The imaginary part is related to damping.

Considering that real part of equation (4.45) for $x < 1$ can be represented as an asymptotic series [38]:

$$\Re Z(x) \simeq -\frac{1}{x}\left(1 + \frac{1}{2\,x^2} + \frac{3}{4\,x^4} + \cdots\right) \tag{4.62}$$

Using equation (4.46) and keeping three terms of expansion:

$$\Re\epsilon = 1 + \Re\chi^e \simeq 1 - \frac{\omega_{pe}^2}{\omega^2}\left(1 + \frac{3}{x_e^2}\right) = 0 \tag{4.63}$$

Which results in Bohm-Gross relation for longitudinal electron plasma waves [10]:

$$\omega^2 = \omega_{pe}^2 + 3\,k^2\,v_{th}^{e\,2} \tag{4.64}$$

Therefore in collective regime, Langmuir waves are observed at $\omega \simeq \omega_{pe}$.

In the limit of low frequencies $\omega \ll \omega_{pi}$, factor $\frac{ZT_e}{T_i}$ determines the scattering pattern. When $\frac{ZT_e}{T_i} < 1$, ion component is dominant and the scattering pattern

reflects ion distribution function. As this factor increases, the ion-acoustic resonance becomes more prominent. In general, ion-acoustic waves are strongly damped unless $\frac{ZT_e}{T_i} \gg 1$.

The electron plasma waves can be used in measurement of electron density and electron temperatures in some regimes, while ion-acoustic waves can provide measurements of electron and ion temperatures [10].

Chapter 5

Results

The dynamic form factor $S(\mathbf{k}, \omega)$ for a Maxwellian plasma, has been derived in Section 4.3 as (4.58). This, alongside (4.59), (4.60) and (4.61) and conditions (2.27) and (2.28) describe the form factor completely. The correlation function of the incident wave was also derived as (3.23). Now that $S(\mathbf{k}, \omega)$ and $C_{EE^*}^G(\mathbf{k}, \omega)$ are known, the convolution (2.52) can be calculated.

It is important to note that $\mathbf{k}$ and ω are calculated inside plasma. The frequencies inside and outside the plasma are the same, however the wave vectors $\mathbf{k_{io}}$ and $\mathbf{k_{so}}$ outside the plasma are related to $\mathbf{k_i}$ and $\mathbf{k_s}$ inside (used in equation (2.28)) as:

$$k_{io,\,so} = \sqrt{k_{i,\,s}^2 + (\frac{\omega_p^2}{c^2})} \tag{5.1}$$

and through dispersion relation

$$\omega_{i,\,s} = k_{io,\,so}\, c \tag{5.2}$$

For electromagnetic wave to propagate, wave number k_i must be real. From equation (5.1):

$$k_i = \sqrt{\omega_i^2 - \omega_p^2}\,/c \tag{5.3}$$

meaning for $\omega_i^2 > \omega_p^2$ wave can propagates inside plasma.

However, the direction of the k vectors remain the same, meaning that scattering angle θ is constant and from equation (2.28):

$$k^2 = k_i^2 + k_s^2 - 2\,k_i\,k_s\,cos\,\theta \tag{5.4}$$

Furthermore, due to dispersion relations, only one of three parameters k_z, $k_\perp$ and ω is independent.

The assumption that plasma is collisionsless is only valid when the collisional mean free path (λ_{ei}) is much larger than the scattering wavelength $(\lambda = 2 * pi\ /\ k)$ i.e $\lambda_{ei}/\lambda \gg 1$. For electron-ion collisions, mean free path is related to electron collision time (τ_e) and electron thermal velocity (v_{th}^e) as:

$$\lambda_{ei} = \tau_e\,v_{th}^e \tag{5.5}$$

The main challenge in the calculation of convolution $S * C$ is the numerical difficulty in evaluation of multiple integrals. Due to the fact that there exist four integration, discretization leads to a large number of multiplications.

Therefore, to reduce the number of independent parameters, two limits for correlation function $C_{EE^*}^G(\mathbf{k}, \omega)$ are considered, corresponding to partial spatial and partial temporal coherence of the probe. For each limit, two examples are presented. In this work the calculations and graphs are performed using MATLAB.

5.1   Partial Temporal Coherence

The first limit is the probe with very large correlation length, $a_0 \to \infty$. Using the identity:

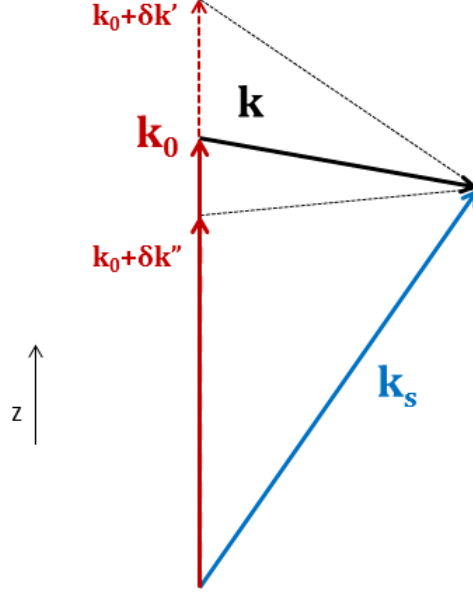$$\frac{1}{\sqrt{2\pi}}\,\lim_{a\to\infty} a\,exp\Big(-\frac{1}{2}a^2 x^2\Big) = \delta(x) \tag{5.6}$$

Figure 5.1: Scattering coordinates in limit $a_0 \rightarrow \infty$

leads to:

$$C_s^G(\mathbf{k'}, \omega') = \lim_{a_0 \rightarrow \infty} C_{EE^*}^G(\mathbf{k'}, \omega')$$

$$= (2\pi)^{7/2} \epsilon_0^2 \tau_0 \, \delta(k'_z - \frac{\omega'}{v_g} + \frac{a_0^2 k'^2_\perp}{2L_R}) \, \delta(k'_\perp) \, exp\big(-\frac{1}{2}\tau_0^2 \omega'^2\big) \qquad (5.7)$$

Equation (5.7) describes the properties of the probe in the limit of a plane wave. Delta function $\delta(k'_\perp)$ indicates no perpendicular component in k-vector of the incident wave, meaning that incident wave propagates parallel to z-axis.

However, pump can be incoherent in time and display frequency range characterized by $1/\tau_0$, where τ_0 is the coherence time. Due to dispersion relation of the pump, ω' and k'_z are related as $\omega' = k'_z v_g$, which is satisfied by delta function $\delta(k'_z - \frac{\omega'}{v_g})$.

Figure 5.1 illustrates probe mean wave number $\mathbf{k_0}$, for an scattered frequency ω_s, corresponding to $\mathbf{k_s}$. $\delta k'$ indicates modification in k_z, while $k_\perp$ remains constant. The convolution means scattered power at ω_s, is the weighed sum of contributions from a range of k-vectors. The k-vectors are confined to

a plane rather than three dimensions and the correlation function has only one independent variable.

Substitution of equation (5.7) in equation (2.52) leads to:

$$S * C_s^G(\mathbf{k}, \omega) =$$

$$(2\pi)^{7/2} \epsilon_0^2 \tau_0 \int \frac{d^3 k'}{(2\pi)^3} \int \frac{d\omega'}{2\pi} \delta(k_z' - \frac{\omega'}{v_g} + \frac{a_0^2 k_\perp'^2}{2L_R}) \, \delta(k_\perp') \, S(\mathbf{k} - \mathbf{k}', \omega - \omega') \; exp(-\frac{1}{2}\tau_0^2 \omega'^2)$$

$$(5.8)$$

Integration over $d^2 k'_\perp$ means replacing $k'_\perp = 0$:

$$S * C_s^G(k_z, k_\perp, \omega) =$$

$$(2\pi)^{7/2} \epsilon_0^2 \tau_0 \int \frac{dk'_z}{(2\pi)^3} \int \frac{d\omega'}{2\pi} \, S(k_z - k'_z, k_\perp, \omega - \omega') \, \delta(k'_z - \frac{\omega'}{v_g}) \; exp(-\frac{1}{2}\tau_0^2 \omega'^2)$$

$$(5.9)$$

Furthermore, integration over dk'_z means replacing $k'_z = \omega'/v_g$:

$$S * C_s^G(k_z, k_\perp, \omega) =$$

$$(2\pi)^{1/2} \epsilon_0^2 \tau_0 \int \frac{d\omega'}{2\pi} \, S(k_z - \omega'/v_g, k_\perp, \omega - \omega') \; exp(-\frac{1}{2}\tau_0^2 \omega'^2)$$

$$(5.10)$$

So the only integration left is over ω', which is significantly less complicated than four integrals involved in the original correlation function. The important factor in the outcome of calculation in (5.10) is parameter τ_0 of the probe. This correlation time can be also interpreted as the duration of a probe pulse.

One interesting case is the limit $\tau_0 \to \infty$, meaning the probe is perfectly coherent (spatially and temporally). Using identity (5.6) and calculation of integral in equation (5.10) leads to:

$$S * C = \epsilon_0^2 \, S(\mathbf{k}, \omega) \qquad (5.11)$$

And the scattered power results in the well-known Thomson scattering cross section. Hence, the effect of correlation function is understood by the comparison of the results of (5.10) and (5.11). The decrease of τ_0 in equation (5.10), broadens the exponential term in frequency space, making its effect more prominent comparing to S.

As an example, parameters are chosen similar to ones used in experiments by C. Rousseaux et al. [39] and [40]. Although unlike our model, in both experiments, plasma waves have been stimulated by Raman scattering [40] or Raman and Brillouin scattering [39]. Plasma properties and scattering parameters are listed in tables 5.1 and 5.2 respectively. Value of α depends on scattered wavelength, the value provided in in table (5.2) is calculated for $\lambda_s = \lambda_i$ to provide an indicator for scattering regime. Assumption of collisionless plasma is valid as $\lambda_{ei}/\lambda \gg 1$.

The ion-acoustic waves and electron plasma waves are shown in figures (5.2) and (5.3) respectively. In these figures, $\omega_{pe} S(\mathbf{k}, \omega)$ are shown as the function of λ_s, the scattered wavelength. These figures are equivalent to (5.11) and are the reference for comparison for examples 1 and 2. For this parameters, we will consider two values for τ_0 as 3×10^{-12} (s) for example 1 and 5×10^{-14} (s) for example 2 and investigate the effect on ion-acoustic and Langmuir waves separately.

Table 5.1: Plasma properties for examples 1 and 2

A	Z	n_e (cm^{-3})	T_e (eV)	T_i (eV)	λ_d (nm)	ω_p (rad/s)
4	2	10^{19}	300	50	40.69	1.8×10^{14}

Table 5.2: Scattering parameters for examples 1 and 2

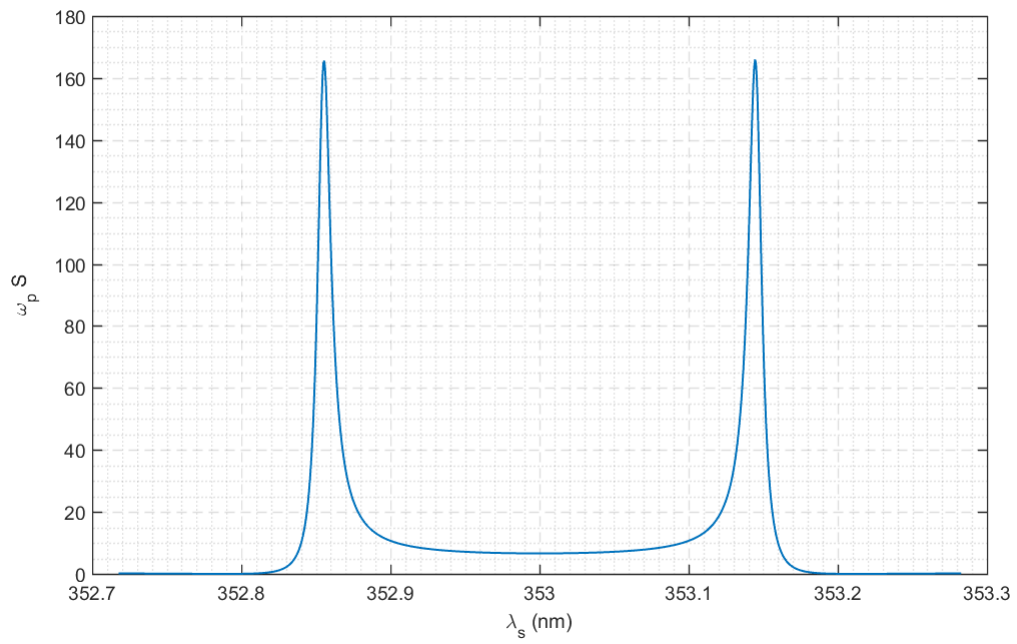| λ_i (nm)	ω_i (rad/s)	θ	α $(\lambda_s = \lambda_i)$	λ_{ei}/λ
353	5.33×10^{15}	63°	1.32	281.44

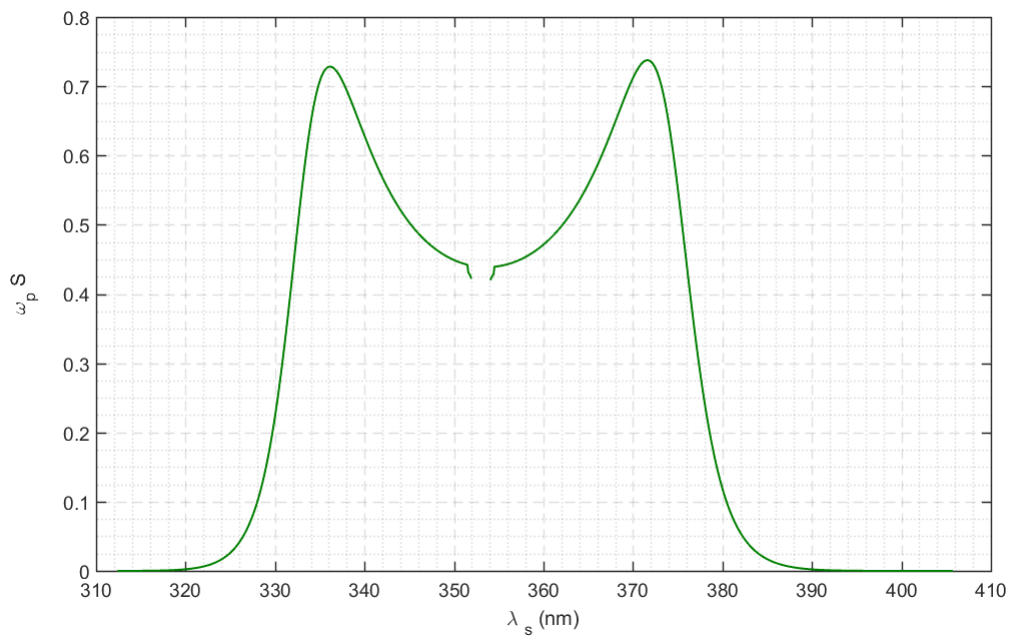Figure 5.2: Ion-acoustic waves, plasma and scattering parameters listed in tables 5.1 and 5.2

Figure 5.3: Electron plasma waves, plasma and scattering parameters listed in tables 5.1 and 5.2
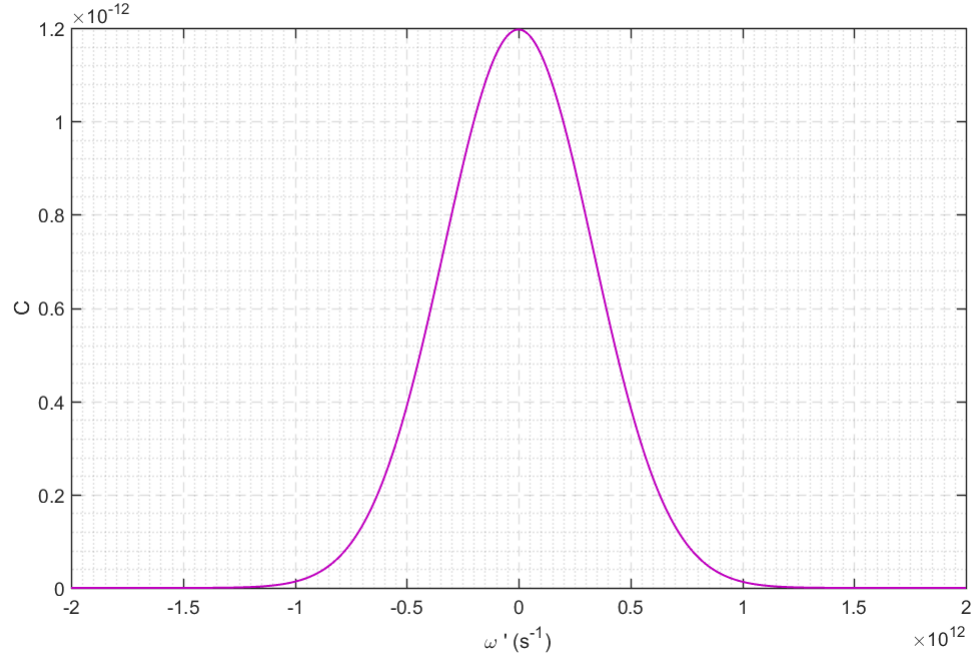
57

Figure 5.4: Example 1 - Probe correlation function

5.1.1 Example 1: $\tau_0 = 3 \times 10^{-12} \, s$

For the first example, we consider the correlation time $\tau_0 = 3 \, ps$. The correlation function $C(\omega')$ is as pictured in figure 5.4. Considering the width of $C(\omega')$ $\sim 2 \times 10^{12} \, s^{-1}$, we expect to mainly see the effect in ion acoustic waves.

The convolution for ion-acoustic waves is shown in figure 5.5 and compared to $S(\mathbf{k}, \omega)$ in figure 5.6. As expected, broadening and decrease in peak of ion acoustic waves are apparent. Meanwhile, the effects on electron plasma waves are negligible.
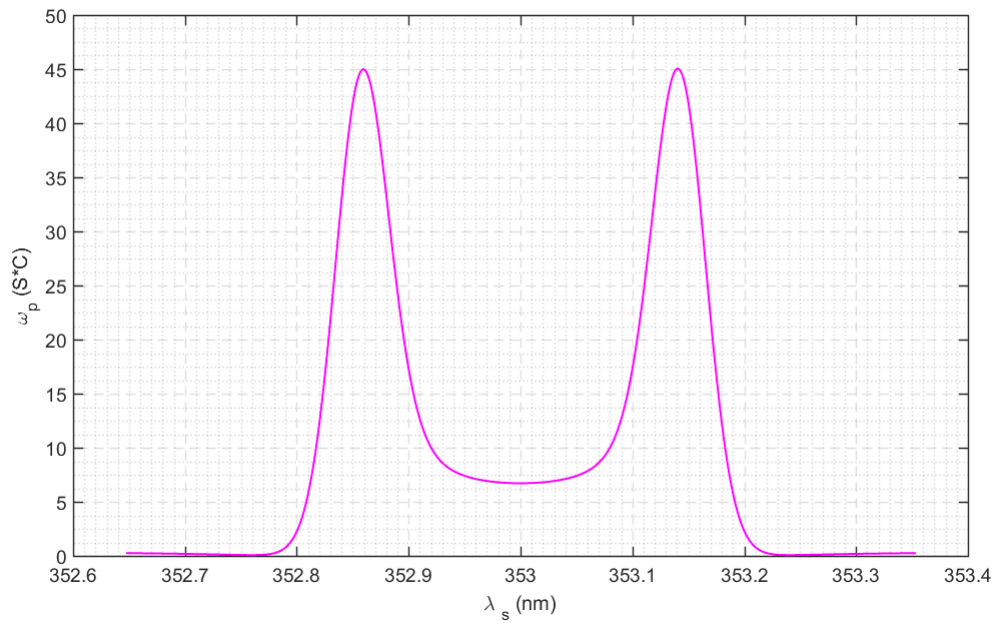
58

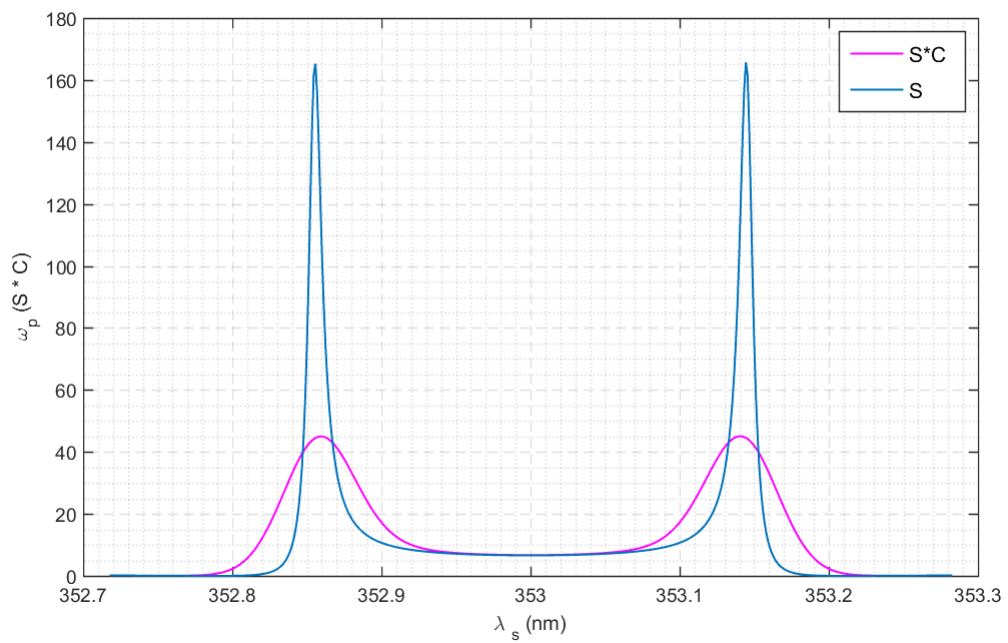Figure 5.5: Example 1 - Convolution for ion-acoustic waves

Figure 5.6: Example 1 - Convolution for ion-acoustic waves compared to $S(\mathbf{k}, \omega)$
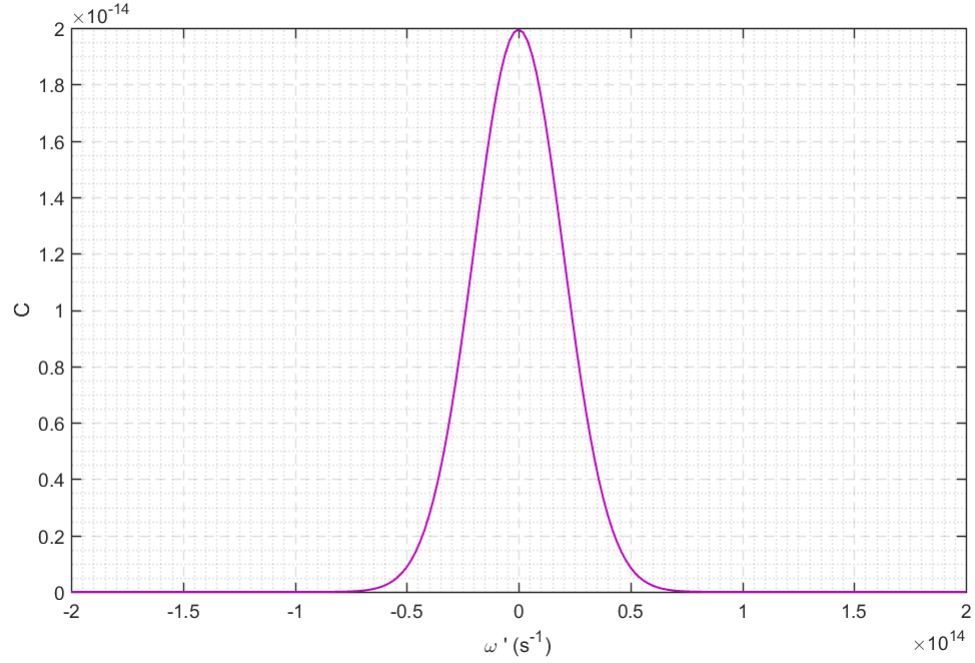
Figure 5.7: Example 2 - Probe correlation function

5.1.2 Example 2: $\tau_0 = 5 \times 10^{-14}$ s

To observe any effect on electron plasma waves, we consider a less coherent probe, i.e. smaller τ_0. Taking $\tau_0 = 5 \times 10^{-14}$ s, correlation function in figure 5.7 is much broader in ω' space. As seen in figure 5.8, ion-acoustic waves disappear. Unlike example 1, electron plasma waves are also affected as shown in figures 5.9 and 5.10.
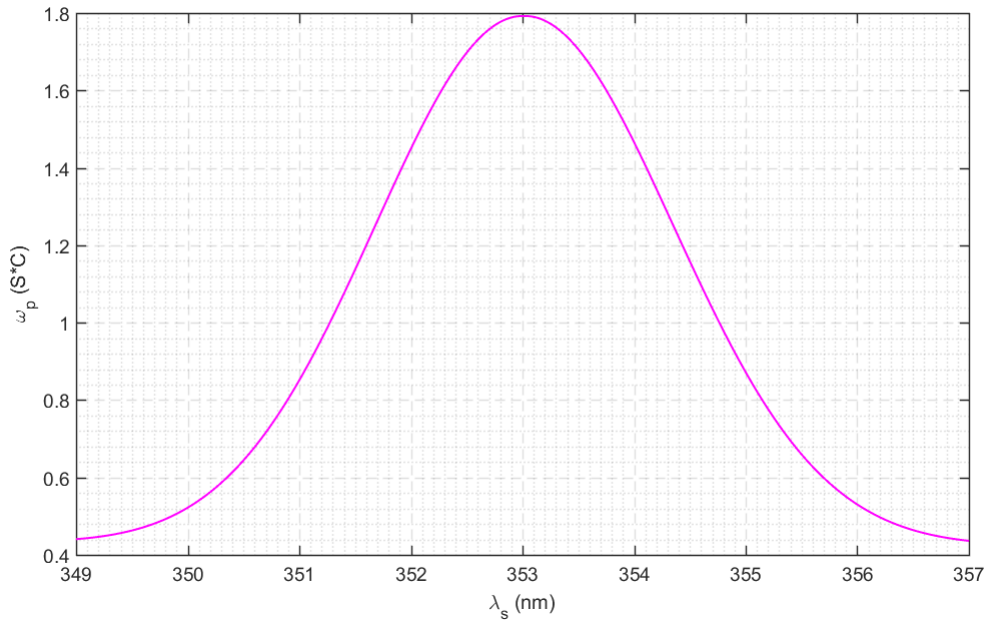
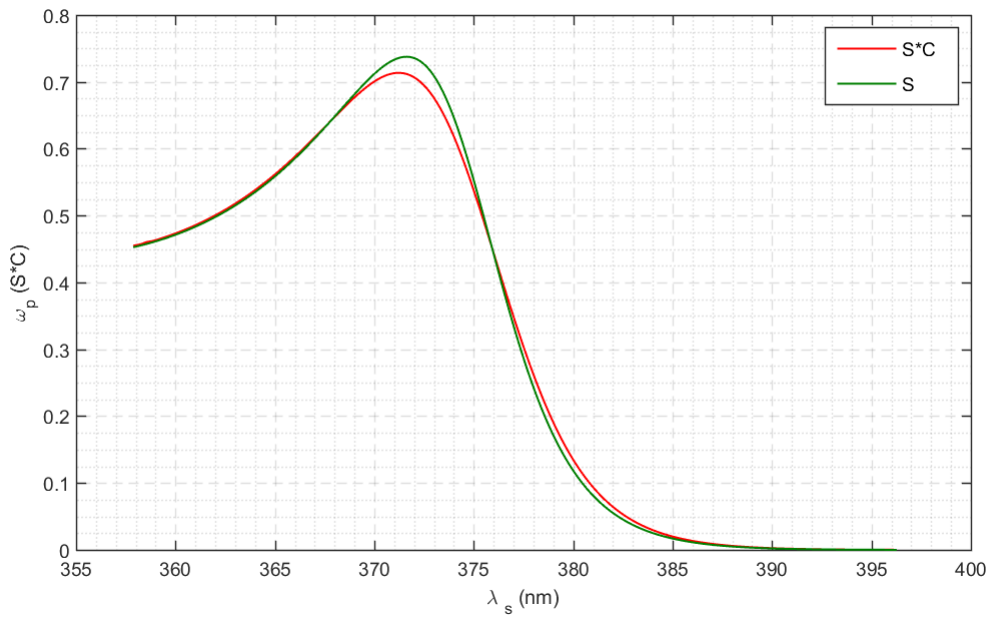Figure 5.8: Example 2 - Convolution for ion-acoustic waves

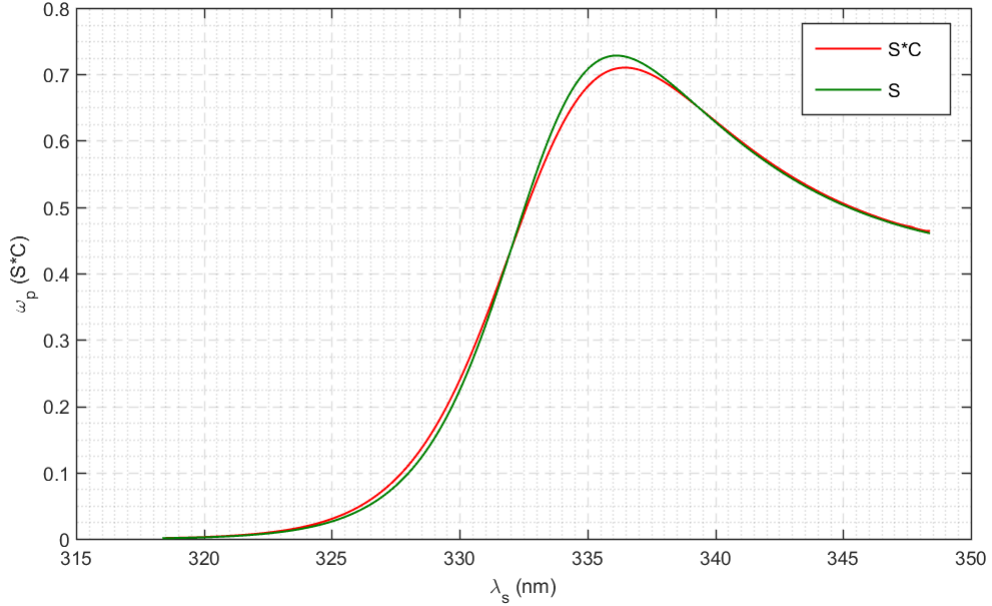Figure 5.9: Example 2 - Convolution for electron plasma wave (R)

61

Figure 5.10: Example 2 - Convolution for electron plasma wave (L)

5.1.3 Deconvolution and Recovery of Ion Acoustic Waves

If τ_0 is sufficiently small, such as case of Example 2, Gaussian correlation function dominates and ion acoustic resonances disappear. In this case, we can use a mathematical process of deconvolution to recover ion acoustic waves. This deconvolution method is widely used in many scientific fields, specially in signal and image processing.

The basis of the deconvolution is convolution theorem. For two functions $f(t)$ and $g(t)$ we have:

$$f(t) = \mathscr{F}^{-1}\Big[F(\nu)\Big] = \int_{-\infty}^{+\infty} F(\nu)\, e^{2\pi i \nu t}\, d\nu \qquad (5.12)$$

$$g(t) = \mathscr{F}^{-1}\Big[G(\nu)\Big] = \int_{-\infty}^{+\infty} G(\nu)\, e^{2\pi i \nu t}\, d\nu \qquad (5.13)$$

where $\mathscr{F}^{-1}$ denotes inverse Fourier transformation. The convolution is:

$$f * g = \int_{-\infty}^{+\infty} g(t') \, f(t - t') \, dt' \tag{5.14}$$

Applying equations (5.12) and (5.13) leads to:

$$f * g = \int_{-\infty}^{+\infty} g(t') \, dt' \int_{-\infty}^{\infty} F(\nu) \, e^{2\pi i \nu (t - t')} \, d\nu \tag{5.15}$$

Reversing the order of integration results in:

$$f * g = \int_{-\infty}^{+\infty} F(\nu) \, e^{2\pi i \nu t} \, d\nu \int_{-\infty}^{+\infty} g(t') \, e^{-2\pi i \nu t'} \, dt' \tag{5.16}$$

which leads to:

$$f * g = \int_{-\infty}^{+\infty} F(\nu) \, G(\nu) \, e^{2\pi i \nu t} \, d\nu = \mathscr{F}^{-1}\left[F(\nu) \, G(\nu)\right] \tag{5.17}$$

Applying Fourier transform to both sides leads to convolution theorem::

$$\mathscr{F}\left[F * G\right] = \mathscr{F}\left[F\right] \cdot \mathscr{F}\left[G\right] \tag{5.18}$$

This means, convolution in frequency domain is multiplication in time domain and vice versa. Therefore, by using Fourier transformation on convoluted function and one of the functions, one should be able to deduct the other function as:

$$f = \mathscr{F}^{-1}\left[\frac{\mathscr{F}[f * g]}{\mathscr{F}[g]}\right] \tag{5.19}$$

Therefore, by applying Fourier transform to correlation function and scattered spectrum, ion acoustic waves can be recovered. Using this method on ion acoustic waves on example 2, figure 5.8, ion acoustic waves were successfully recovered as figure 5.2.

Figure 5.11: Scattering coordinates in limit $\tau_0 \to \infty$

5.2 Partial Spacial Coherence

The second limit corresponds to very long correlation time, $\tau_0 \to \infty$. Using identity (5.6) leads to:

$$\lim_{\tau_0 \to \infty} C^G_{EE*}(\mathbf{k}',\omega') = (2\pi)^3 \epsilon_0^2 a_0^2\, \delta(k'_z - \frac{\omega'}{v_g} + \frac{a_0^2 k'^2_\perp}{2L_R})\, \delta(\omega')\, exp(-\frac{1}{2}a_0^2 k'^2_\perp)\ \ (5.20)$$

The delta function $\delta(\omega')$ in equation (5.20) essentially means that the probe is monochromatic. As seen in figure 5.11, this means that the only change is in the direction of $\mathbf{k_0}$; therefore the k-vector sweeps part of a sphere with radius k_0. The other delta function, $\delta(k' + \frac{a_0^2 k'^2_\perp}{2L_R})$ is consistent with paraxial approximation and corresponds to $k_0 = constant$.

Equation (5.20) is then substituted in equation (2.52):

$$S * C_t^G(\mathbf{k}, \omega) =$$

$$(2\pi)^3 \epsilon_0^2 a_0^2 \int \frac{d^3 k'}{(2\pi)^3} \int \frac{d\omega'}{2\pi} \, S(\mathbf{k} - \mathbf{k'}, \omega - \omega') \, \delta(k'_z - \frac{\omega'}{v_g} + \frac{a_0^2 k'^2_\perp}{2L_R}) \, \delta(\omega) \, exp(-\frac{1}{2} a_0^2 k'^2_\perp)$$

Integration over ω' means replacing $\omega' = 0$:

$$S * C_t^G(\mathbf{k}, \omega) =$$

$$(2\pi)^3 \epsilon_0^2 a_0^2 \int \frac{d^3 k'}{(2\pi)} \, S(\mathbf{k} - \mathbf{k'}, \omega) \, \delta(k'_z + \frac{a_0^2 k'^2_\perp}{2L_R}) \, exp(-\frac{1}{2} a_0^2 k'^2_\perp)$$

$$(5.21)$$

Integration over k'_z replaces $k'_z = -\frac{a_0^2 k'^2_\perp}{2L_R}$ leading to two dimensional integral:

$$S * C_t^G(k_z, k_\perp, \omega) =$$

$$(2\pi)^{-1} \epsilon_0^2 a_0^2 \int d^2 \mathbf{k'}_\perp \, S(k_z + \frac{a_0^2 k'^2_\perp}{2L_R}, \mathbf{k}_\perp - \mathbf{k'}_\perp, \omega) \, exp(-\frac{1}{2} a_0^2 k'^2_\perp)$$

Table 5.3: Plasma properties for examples 3 and 4

A	Z	$n_e \ (cm^{-3})$	$T_e \ (eV)$	$T_i \ (eV)$	$\lambda_d \ (nm)$	$\omega_p \ (rad/s)$
190	50	10^{22}	1000	1000	2.35	5.6×10^{15}

Table 5.4: Scattering parameters for examples 3 and 4

$\lambda_i \ (nm)$	$\omega_i \ (rad/s)$	θ	$\alpha \ (\lambda_s = \lambda_i)$	λ_{ei}/λ
1.6	1.18×10^{18}	5°	1.24	34.45

For Example 3 and 4, we consider a plasma and pump with properities listed in tables 5.3 and 5.4 respectively, varying a_0 as $a_0 = 1.7 \times 10^{-7}$ m and $a_0 = 1.7 \times 10^{-8}$ m. Plasma can be considered collsionless as $\lambda_{ei}/\lambda \gg 1$. This is an example of x-ray laser beam that is Thomson scattered from dense plasma. Such a plasma is opaque to visible radiation and x-ray pulse generated by free electron lacks transverse (spatial) coherence [41]. The ion-acoustic waves and
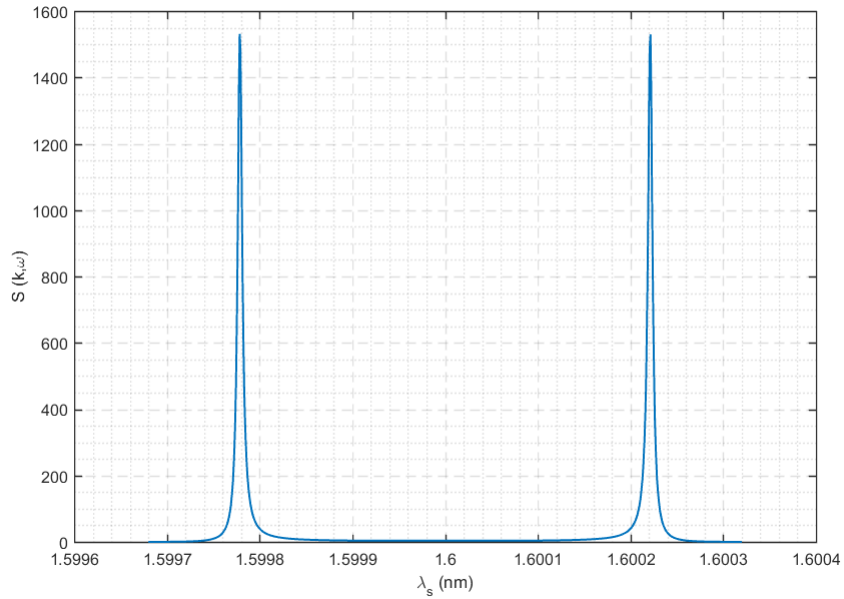
Figure 5.12: Ion acoustic waves, scattering with parameters listed in tables 5.3 and 5.4

electron plasma waves for these parameters are seen in figures 5.12 and 5.13 respectively.

5.2.1 Example 3: $a_0 = 1.7 \times 10^{-7}\ m$

The correlation function is two dimensional as seen in figure 5.14. The convolution for ion acoustic waves are seen in figure 5.15. Figures 5.16 and 5.17 show the broadening effect for each ion acoustic wave more accurately. For electron plasma waves no change is observed.
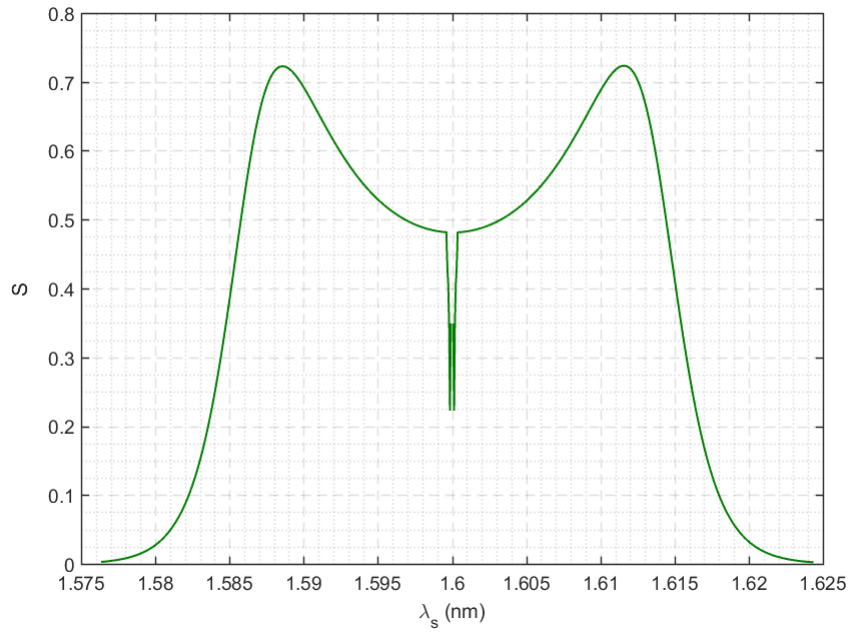
Figure 5.13: Electron plasma waves, scattering with parameters listed in tables 5.3 and 5.4
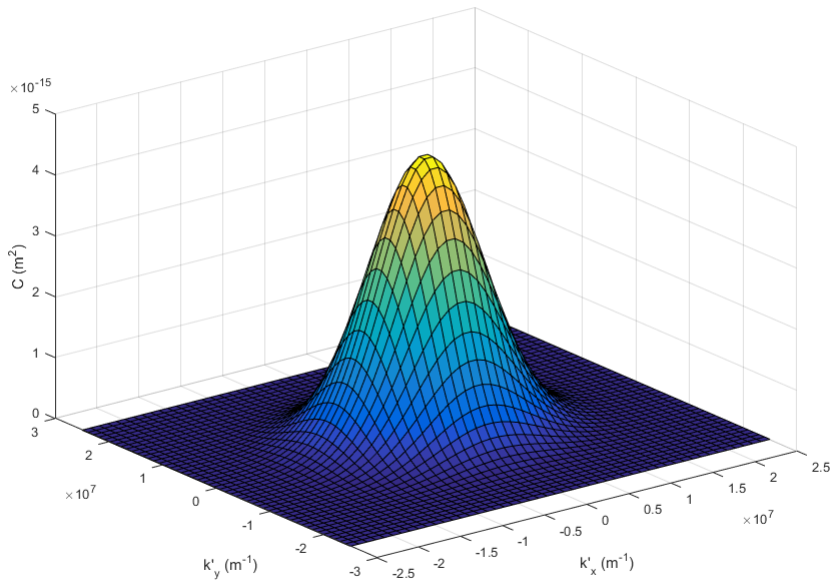
Figure 5.14: Example 3 - Probe correlation function
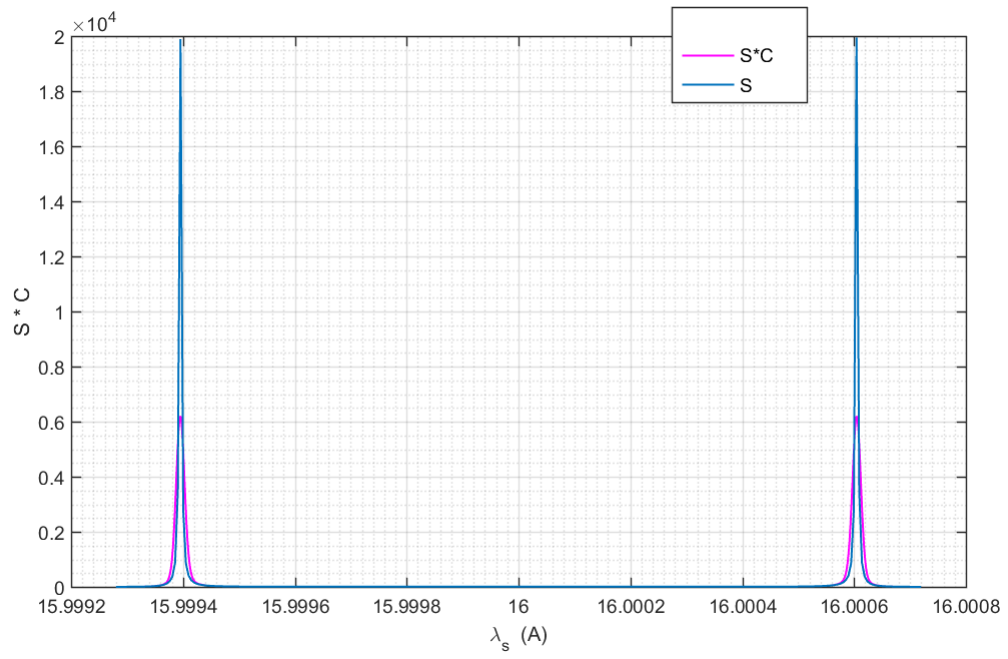
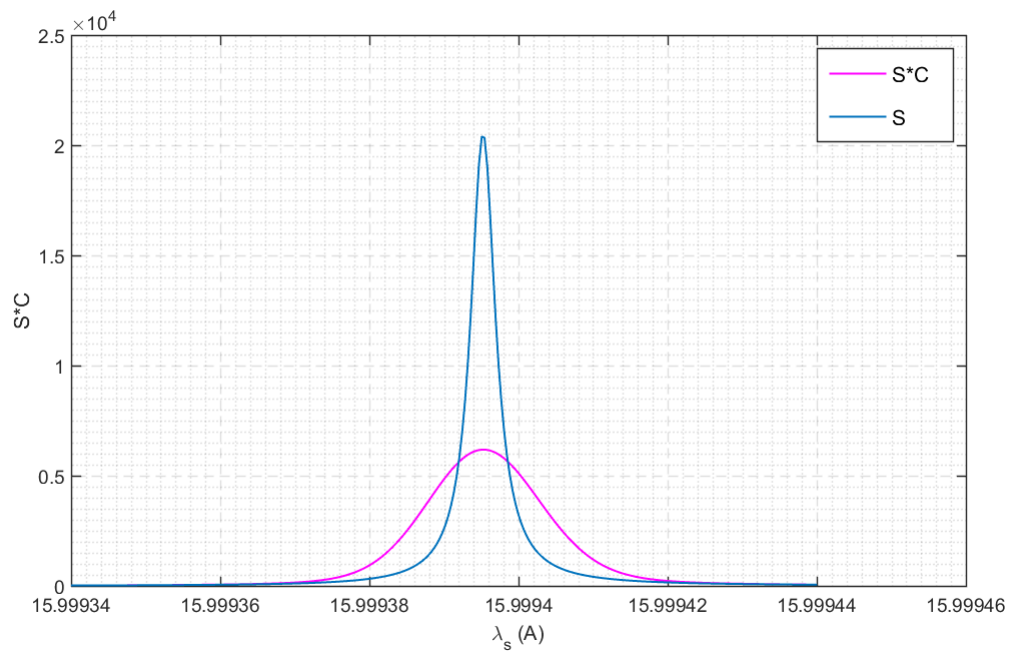Figure 5.15: Example 3 - Convolution for ion-acoustic waves

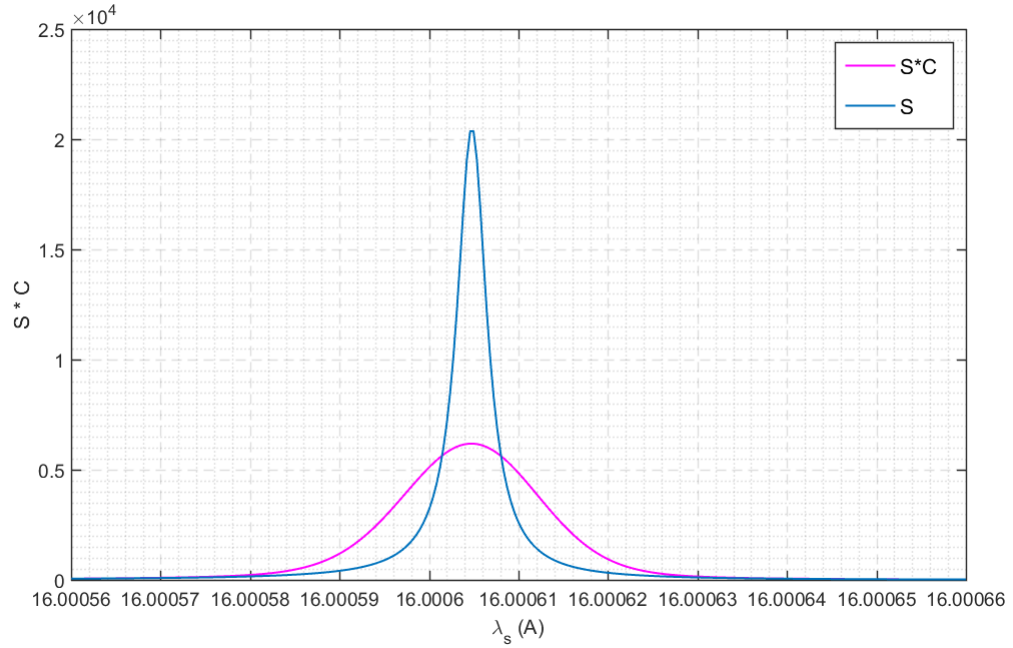Figure 5.16: Example 3 - Convolution for ion-acoustic wave (L)

Figure 5.17: Example 3 - Convolution for ion-acoustic wave (R)

5.2.2 Example 4: $a_0 = 1.7 \times 10^{-8} \; m$

Since a_0 is smaller than value for example 3, the correlation function in figure 5.18 is broader.

Ion acoustic waves are shown in figure 5.19 and separately in figures 5.20 and 5.21. Electron plasma waves are as well affected as shown in 5.22 and 5.23.
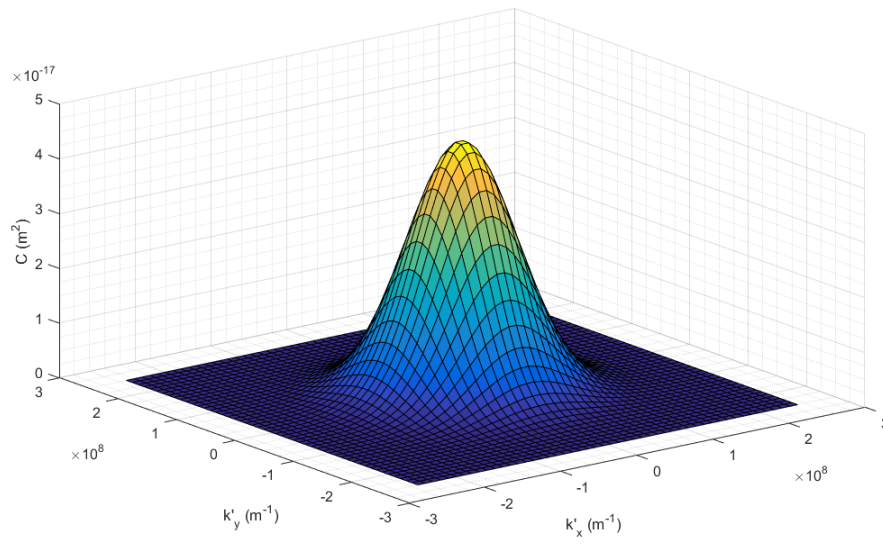
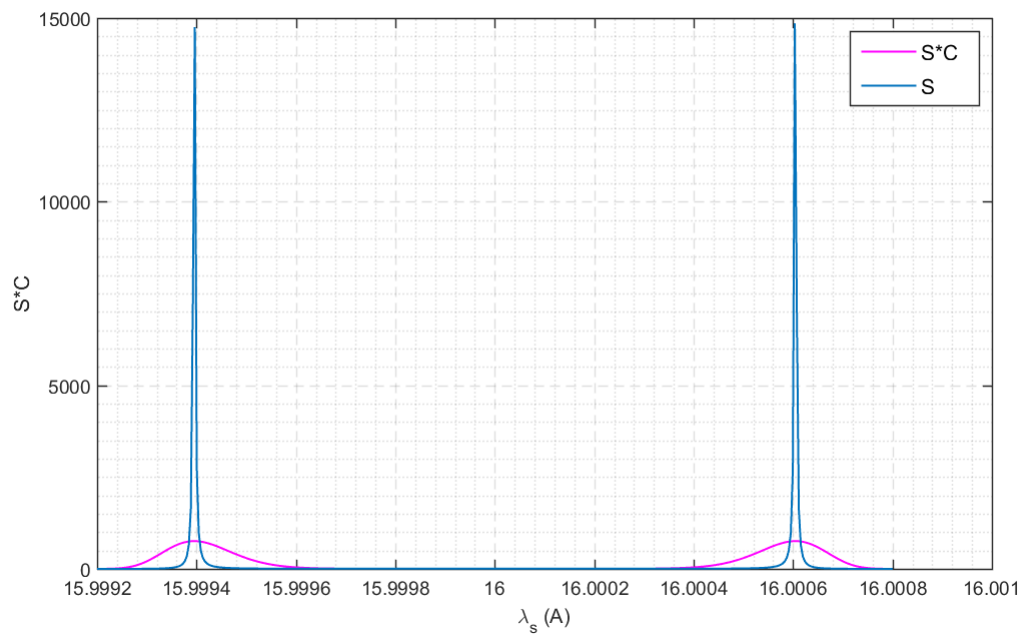Figure 5.18: Example 4 - Probe correlation function

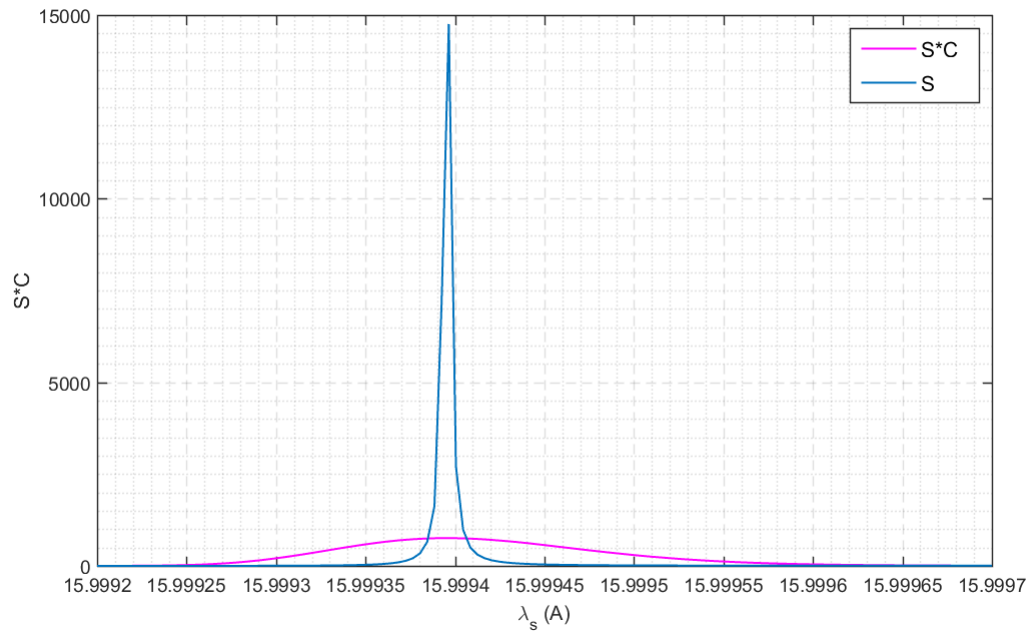Figure 5.19: Example 4 - Convolution for ion acoustic waves

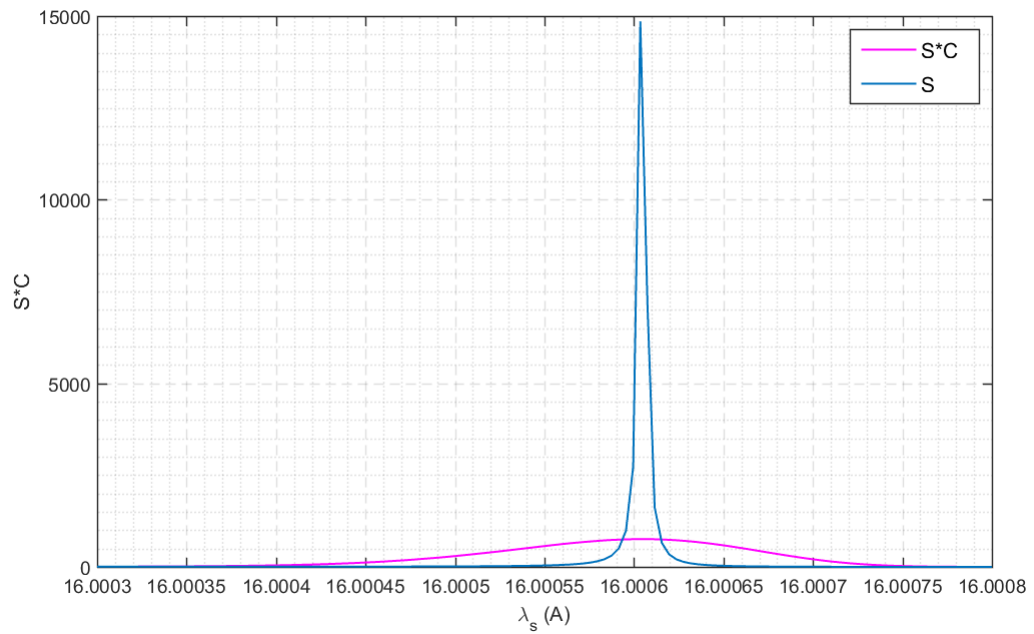Figure 5.20: Example 4 - Convolution for ion acoustic wave (L)

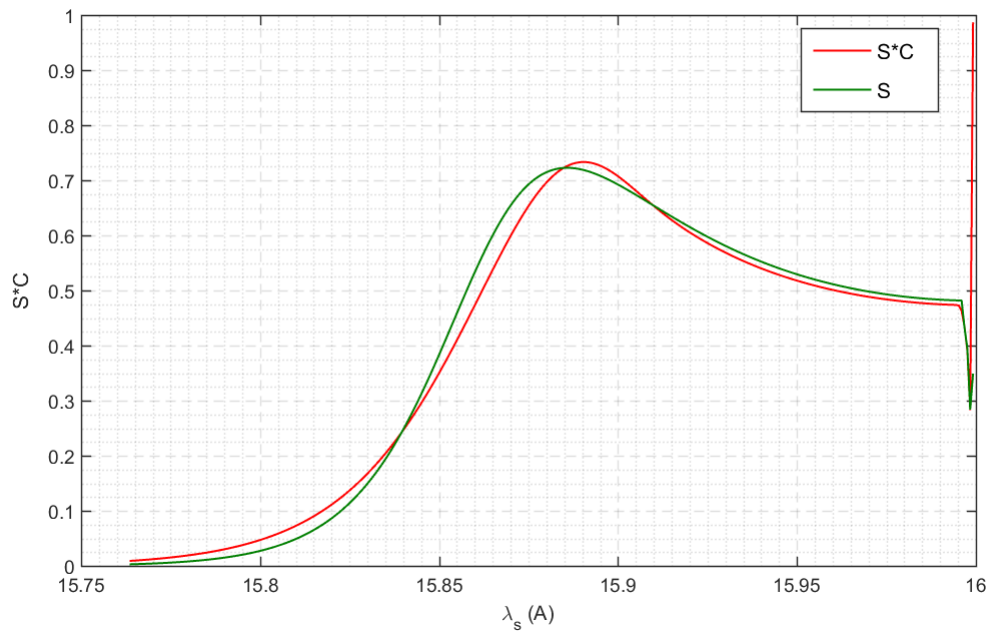Figure 5.21: Example 4 - Convolution for ion acoustic wave (R)

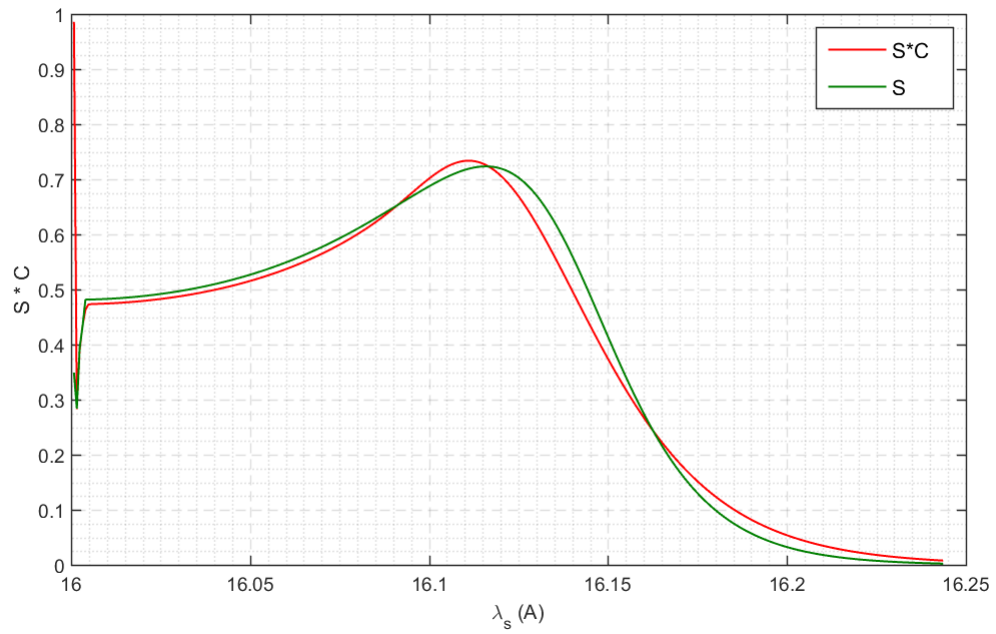Figure 5.22: Example 4 - Convolution for electron plasma wave (L)

Figure 5.23: Example 4 - Convolution for electron plasma wave (R)

Chapter 6

Summary and Conclusions

In Chapter 2, using basic electromagnetic theory we discussed fundamentals of Thomson Scattering. Starting from a single charge Doppler shift is then explained. Dynamic form factor $S(\mathbf{k}, \omega)$ and probe correlation function are then related to the scattering power.

In Chapter 3, correlation function, temporal and spatial coherence are reviewed. Then using paraxial wave approximation, Gaussian correlation function $C_{EE^*}^G(\mathbf{k}, \omega)$ is calculated.

In Chapter 4, dressed test particle method is used to establish relationship between dynamic form factor and plasma susceptibility. Dynamic form factor is then derived for a plasma with Maxwellian velocity distribution. Ion acoustic and electron plasma waves are discussed for different parameters.

Using derived functions, two limiting cases for partial coherence are discussed in Chapter 5. First case being spatial coherence characterized by very large coherence length $(a_0 \rightarrow \infty)$ but finite coherence time (τ_0) or a non monochromatic probe. In this case, problem is reduced to a one dimensional convolution. Then using convolution theorem, a method is proposed to recover ion acoustic wave spectra.

Second case discussed was of a monochromatic probe (temporal coherence), with finite coherence length. The calculations were involved with a two dimen-

sional integral.

For each case, MATLAB programs were developed to calculate the scattered power spectrum. To show the results, two examples were provided for each case. As expected, the effect of probe incoherence was seen as broadening in both ion acoustic and electron plasma waves. The less coherent the probe (smaller τ_0 or a_0), the more prominent the effect of broadening. This can be seen by comparing Example 1 with Example 2 and Example 3 with Example 4. Predictably, the lower frequency resonances corresponding to ion acoustic waves are more prone to effects of probe partial incoherence, as in Example 1 and Example 3, they are broadened while electron plasma waves are unaffected. Also, as expected the peaks move toward the center due to range of probe wavelength.

The models proposed are capable of detecting the effect of spatial and temporal partial coherence for any plasma and probe parameters. However, discretization parameters must be adjusted to suit the particular parameters.

The plasma modeled was homogeneous with no temperature ingredient and velocity distribution was considered Maxwellian. Also in deconvolution, the effects of any noise was disregarded. As suggestion to future improvement in the model, partial temporal and spatial coherence may be combined, rather than considering only one type of partial coherence. Furthermore, plasma may be considered magnetized. Also, this model was inspired by experimental observations, but actual comparison with experimental data was not made. Therefore, future work could involve comparison of the results from this model with experimental data.

Bibliography

[1] John David Jackson. *Classical electrodynamics*. Wiley, (1999).

[2] Irving Langmuir. *Oscillations in ionized gases*. Proceedings of the National Academy of Sciences, 14(**8**):627, (1928).

[3] William Crookes. *On radiant matter*. Journal of the Franklin Institute, 108(**5**):305, (1879).

[4] *Thomson, Joseph John*. Xl. cathode rays. The London, Edinburgh, and Dublin Philosophical Magazine and Journal of Science, 44(**269**):293, (1897).

[5] Alexander Piel and Michael Brown. *Plasma Physics: An Introduction to Laboratory, Space, and Fusion Plasmas*. Physics Today, 64(**6**):55, (2011).

[6] Richard Fitzpatrick. *Plasma physics: an introduction*. CRC Press, (2014).

[7] Clifford W. Mendel Jr. and Edl Schamiloglu. *Plasma Diagnostic Techniques*. the Encyclopedia of Physical Science and Technology, 12:391, (2002).

[8] Ian H. Hutchinson. *Principles of plasma diagnostics*. Cambridge University Press, (1990).

[9] AA Ovsyannikov. *Plasma diagnostics*. Cambridge Int. Science Publishing, (2000).

[10] John Sheffield, Dustin Froula, Siegfried H. Glenzer, and Neville C. Luhmann Jr. *Plasma scattering of electromagnetic radiation: theory and measurement techniques.* Academic press, (2010).

[11] John William Strutt Baron Rayleigh. *On the scattering of light by small particles.* (1871).

[12] Akira Ishimaru. *Wave propagation and scattering in random media*, volume 2. Academic press New York, (1978).

[13] William E. Gordon. *Incoherent scattering of radio waves by free electrons with applications to space exploration by radar.* Proceedings of the IRE, 46(**11**):1824, (1958).

[14] KL Bowles. *Observation of vertical-incidence scatter from the ionosphere at 41 Mc/sec.* Phys. Rev. Lett., 1(**12**):454, (1958).

[15] VC Pineo, LG Kraft, and HW Briscoe. *INCOHERENT BACKSCATTER FROM THE IONOSPHERE OBSERVED AT 440 MC-S.* In Journal of Geophysical Research, volume 65, page 2517, (1960).

[16] G. Fiocco and E. Thompson. *Thomson scattering of optical radiation from an electron beam.* Phys. Rev. Lett., 10(**3**):89, (1963).

[17] NJ Peacock, DC Robinson, MJ Forrest, PD Wilcock, and VV Sannikov. *Measurement of the electron temperature by Thomson scattering in tokamak T3.* Nature, 224(**5218**):488, (1969).

[18] Deviderjit Singh Sivia. *Elementary scattering theory: for X-ray and neutron users.* Oxford University Press, (2011).

[19] Vinod Krishan. *Plasmas.* Cambridge University Press, (2014).

[20] Richard H. Milburn. *Electron scattering by an intense polarized photon field.* Phys. Rev. Lett., 10(**3**):75, (1963).

[21] FR Arutyunian and VA Tumanian. *The Compton effect on relativistic electrons and the possibility of obtaining high energy beams.* Phys. Let., 4 (**3**):176, (1963).

[22] David Jeffrey Griffiths and Reed College. *Introduction to electrodynamics*, volume 3. Prentice Hall Upper Saddle River, NJ, (1999).

[23] Oleg D. Jefimenko. *Electricity and magnetism.* Appleton-Century-Crofts, (1966).

[24] Edwin E. Salpeter. *Electron density fluctuations in a plasma.* Phys. Rev. Lett., 120(**5**):1528, (1960).

[25] Werner Lauterborn, Thomas Kurz, Martin Wiesenfeldt, and Minhua Liang. *Coherent Optics: Fundamentals and Applications.* Optical Engineering, 35(**6**):1800, (1996).

[26] Bahaa EA Saleh, Malvin Carl Teich, and Bahaa E. Saleh. *Fundamentals of photonics*, volume 22. Wiley New York, (1991).

[27] Joseph W Goodman. *Statistical optics.* John Wiley & Sons, (2015).

[28] Olga Korotkova. *Random light beams: theory and applications.* CRC press, (2013).

[29] Max Born and Emil Wolf. *Principles of optics: electromagnetic theory of propagation, interference and diffraction of light.* CUP Archive, (2000).

[30] Emil Wolf. *Introduction to the Theory of Coherence and Polarization of Light.* Cambridge University Press, (2007).

[31] Edward L. O'Neill. *Introduction to statistical optics.* Courier Corporation, (2004).

[32] Joseph H. Eberly Peter W. Milonni. *Laser Physics.* John Wiley & Sons, (2010).

[33] Heinrich Hora and Helmut J Schwarz. *Laser Interaction and Related Plasma Phenomena.* Nuclear Fusion, 17(**1**):165, (1977).

[34] AV Brantov, V. Yu Bychenkov, VT Tikhonchuk, W. Rozmus, and VK Senecha. *Plasma fluctuations driven by a randomized laser beam.* Physics of Plasmas, 6(**8**):3002, (1999).

[35] Kyōji Nishikawa and Masahiro Wakatani. *Plasma Physics: basic theory with fusion applications*, volume 8. Springer Science & Business Media, (2013).

[36] Donald Gary Swanson. *Plasma kinetic theory.* CRC Press, (2008).

[37] Setsuo Ichimaru. *Statistical plasma physics.* Addison-Wesley, (2004).

[38] Thomas James Morrow Boyd and Jeffrey John Sanderson. *The physics of plasmas.* Cambridge University Press, (2003).

[39] C Rousseaux, L Gremillet, M Casanova, P Loiseau, M Rabec Le Gloahec, SD Baton, F Amiranoff, JC Adam, and A Héron. *Transient development of backward stimulated Raman and Brillouin scattering on a picosecond time scale measured by subpicosecond Thomson diagnostic.* Phys. Rev. Lett., 97(**1**):015001, (2006).

[40] C. Rousseaux, SD Baton, D. Bénisti, L. Gremillet, JC Adam, A. Héron, DJ Strozzi, and F Amiranoff. *Experimental evidence of predominantly transverse electron plasma waves driven by stimulated Raman scattering of picosecond laser pulses.* Phys. Rev. Lett., 102(**18**):185003, (2009).

[41] IA Vartanyants, A. Singer, AP Mancuso, OM Yefanov, A. Sakdinawat, Y. Liu, E. Bang, Garth J. Williams, G. Cadenazzi, B. Abbey, et al. *Coherence properties of individual femtosecond pulses of an x-ray free-electron laser.* Phys. Rev. Lett., 107(**14**):144801, (2011).